

Hygroscopic properties of the ambient aerosol in southern Sweden

E. O. Fors et al.

Hygroscopic properties of the ambient aerosol in southern Sweden – a two year study

E. O. Fors, E. Swietlicki, B. Svenningsson, A. Kristensson, G. P. Frank, and M. Sporre

Lund University, Department of Physics, Division of Nuclear Physics, Lund University, Lund, Sweden

Received: 31 January 2011 – Accepted: 15 February 2011 – Published: 23 February 2011

Correspondence to: E. O. Fors (erik.fors@nuclear.lu.se)

Published by Copernicus Publications on behalf of the European Geosciences Union.

Title Page

Abstract

Introduction

Conclusions

References

Tables

Figures

⏪

⏩

◀

▶

Back

Close

Full Screen / Esc

Printer-friendly Version

Interactive Discussion

Abstract

The hygroscopic growth of the atmospheric aerosol is a critical parameter for quantifying the anthropogenic radiative forcing. Until now, there has been a lack of long term measurements due to limitations in instrumental techniques. In this work, for the first time the seasonal variation of the hygroscopic properties of a continental background aerosol has been described, based on more than two years of continuous measurements. In addition to this, the diurnal variation of the hygroscopic growth has been investigated, as well as the seasonal variation in CCN concentration. These physical properties of the aerosol have been measured with a Hygroscopic Tandem Differential Mobility Analyzer (H-TDMA), a Differential Mobility Particle Sizer (DMPS), and a Cloud Condensation Nuclei Counter (CCNC). The results show that smaller particles are generally less hygroscopic than larger ones, and that there is a clear difference in the hygroscopic properties between the Aitken and the accumulation mode. A seasonal cycle was found for all particle sizes. In general, the average hygroscopic growth is lower during wintertime, due to an increase in the relative abundance of less hygroscopic or hydrophobic particles. Monthly averages showed that the hygroscopic growth factors of the two dominating hygroscopic modes (one barely hygroscopic and one more hygroscopic) were relatively stable. The hygroscopic growth additionally showed a diurnal cycle, with higher growth factors during day time. CCN predictions based on H-TDMA data underpredicted the activated CCN concentration with 7% for 1% water supersaturation (s). The underprediction increases with decreasing s , most likely due to a combination of measurement and modeling uncertainties. It was found that although the aerosol is often externally mixed, recalculating to an internal mixture with respect to hygroscopicity did not change CCN parameterizations significantly.

Hygroscopic properties of the ambient aerosol in southern Sweden

E. O. Fors et al.

Title Page

Abstract

Introduction

Conclusions

References

Tables

Figures



Back

Close

Full Screen / Esc

Printer-friendly Version

Interactive Discussion



1 Introduction

The hygroscopic properties of atmospheric aerosols are of utmost importance for the climate. As aerosol particles move around the atmosphere, they continuously interact with the surrounding water vapour, changing in size with the relative humidity (RH). As the light scattering properties of particles are highly dependent on particle size, the hygroscopicity of the aerosol at subsaturated conditions will have great implications for the light scattering of the atmosphere (Fierz-Schmidhauser et al., 2010; McFiggans et al., 2006) The light scattering of the aerosol is commonly called “the direct aerosol climate effect” and is believed to cool the atmosphere, an effect that is enhanced by anthropogenic emissions (Solomon, 2007).

The particle-water vapour interaction also plays a vital role in cloud formation, as the particles provide a surface on which to condense when the air is saturated with water. At a water vapour saturation ratio just above 100%, the particles leave the equilibrium domain and start to grow unrestrained as long as water vapour is available for condensation. The particles are said to *activate* into cloud droplets, often growing from 100 nm to 10 μm in a few hours. The number of activated particles in a cloud is highly dependent on the hygroscopic properties of the particles (McFiggans et al., 2006) as well as the size distribution of the aerosol (Dusek et al., 2006) which determines how many activated cloud droplets will form for a given supersaturation (s) ratio. This in turn affects both the reflective properties and precipitation pattern of the cloud (Rosenfeld, 1999, 2000), effects which also are believed to exert a cooling of the atmosphere, and which are known as the first and second aerosol indirect effects.

To quantify the water uptake at subsaturated conditions, the concept of hygroscopic diameter growth factor (GF) is commonly used where the GF is defined according to

$$\text{GF} = \frac{D_w}{D_p} \quad (1)$$

where D_w is the wet particle diameter at a given RH and D_p is the dry diameter of the particle. At subsaturated conditions (RH < 100%), particles rapidly reach equilibrium

Hygroscopic properties of the ambient aerosol in southern Sweden

E. O. Fors et al.

Title Page

Abstract

Introduction

Conclusions

References

Tables

Figures

⏪

⏩

◀

▶

Back

Close

Full Screen / Esc

Printer-friendly Version

Interactive Discussion



with the surrounding atmosphere, with GFs ranging between 1 and ~2.1 at 90% RH, where 1 represents completely hydrophobic particles, such as fresh soot, and ~2.1 represents sea salt particles (Swietlicki et al., 2008).

Hygroscopic measurements of atmospheric aerosol particles have been carried out for many years, with Sekigawa (1983) and Rader and McMurry (1986) doing pioneering work in using the measurement principle of two DMAs in series with a humidification conditioning unit in between on an atmospheric aerosol. This setup is commonly known as the Hygroscopic Tandem Differential Mobility Analyzer (H-TDMA). Since the first measurements, there have been a multitude of measurement campaigns using H-TDMAs in various environments all over the globe. Results from these measurements show that the hygroscopicity of a particle is highly dependent on the source and physicochemical age of the particle.

The hygroscopic growth can be subdivided into four classes with respect to GF at 90% RH. For 100 nm dry particles diameter the boundaries are: Nearly Hydrophobic (NH; GF = 1.0–1.11), Less Hygroscopic (LH; GF = 1.11–1.33), More Hygroscopic (MH; GF = 1.33–1.85) and Sea Salt (GF > 1.85) (Swietlicki et al., 2008). Often the ambient aerosol is externally mixed, meaning that for any given size, there are particles present in two or more of the hygroscopic classes, with different GFs dependent on air mass origin and different chemical age. However, the degree of external mixture is dependent both on location and on size.

For previous H-TDMA measurements, the occurrence of external mixtures varies a lot between different measurement campaigns. The aerosol tends to be less externally mixed for Aitken mode particles than for accumulation mode particles (Swietlicki et al., 2008). This might be explained by the fact that some of the larger particles have been cloud processed, during which they absorbed soluble gases such as SO₂, H₂SO₄, HNO₃ or NH₃. When the particles dry out, soluble ions tend to stay in the particle phase, increasing its solubility.

On the other hand, also the smaller particles are often externally mixed. This is most likely due to a combination of different sources and different age. Small particles tend

Hygroscopic properties of the ambient aerosol in southern Sweden

E. O. Fors et al.

Title Page

Abstract

Introduction

Conclusions

References

Tables

Figures

⏪

⏩

◀

▶

Back

Close

Full Screen / Esc

Printer-friendly Version

Interactive Discussion

though diurnal cycles were observed, no clear seasonal trend could be observed over a 13 month measurement period in the Swiss free troposphere.

In this work, more than two years of H-TDMA, size distribution and CCNC data are presented, for the first time revealing the annual cycle of the hygroscopic properties at subsaturated conditions as well as the CCN concentrations of a European background aerosol. The aims of this work were

1. To characterize the hygroscopic properties of the aerosol at Vavihill, including the diurnal and seasonal variation of the hygroscopic growth.
2. To quantify how well we are able to predict CCN concentrations using size distribution and H-TDMA data.
3. To parameterize seasonal CCN concentration as function of supersaturation for all four seasons.

2 Methods

The measurements included in this work were carried out at the EMEP/EUSAAR field station Vavihill (56°01' N, 13°09' E, 172 m a.s.l.), which is situated in a rural environment in the southern part of Sweden (Kristensson et al., 2008). The aerosol was sampled through a PM₁₀ inlet, excluding all particles with an aerodynamic diameter larger than 10 µm. The temperature inside the measurement station was kept constant with air conditioning at 21 ± 2 °C.

2.1 H-TDMA

The hygroscopic properties at subsaturated conditions were measured with an H-TDMA constructed at Lund University which was specifically constructed for long term measurements, in accordance with the design and operation criteria decided within the EU FP6 Infrastructure Project EUSAAR. The aerosol was dried and charged with

Hygroscopic properties of the ambient aerosol in southern Sweden

E. O. Fors et al.

Title Page

Abstract

Introduction

Conclusions

References

Tables

Figures



Back

Close

Full Screen / Esc

Printer-friendly Version

Interactive Discussion



Hygroscopic properties of the ambient aerosol in southern Sweden

E. O. Fors et al.

[Title Page](#)[Abstract](#)[Introduction](#)[Conclusions](#)[References](#)[Tables](#)[Figures](#)[Back](#)[Close](#)[Full Screen / Esc](#)[Printer-friendly Version](#)[Interactive Discussion](#)

an ^{85}Kr diffusion charger before it entered the first DMA (DMA1), a Vienna type, 28 cm long, which was housed in an insulated box at a well defined temperature, typically 20°C . Here a fixed voltage was applied, corresponding to a certain dry size, or more precisely to a certain electrical mobility. After DMA1, the aerosol was quasi-monodisperse, meaning that it had a mobility distribution corresponding to the transfer function of DMA1. The flow ratio between the aerosol and the sheath flow was set to $1:10\text{ l min}^{-1}$, to minimize broadening of the spectrum.

After DMA1, the aerosol passed through Gore-TexTM tubing, with temperature controlled water flowing on the outside of the membrane in opposite direction. The water migration through the membrane was controlled by the temperature of the water. After this conditioning unit, the aerosol flowed into a second housing, with a temperature 2 K lower than the first. Since the saturation vapor pressure of the water decreases with temperature, the RH increased before it entered the second DMA (DMA2) and the use of a closed loop for the sheath and excess flow made the RH inside DMA2 asymptotically approach the RH of the aerosol entering the DMA.

By ensuring a well controlled temperature, the DMA2 RH was kept at $90 \pm 0.1\%$. Since the particles have grown in the humidifier, the voltage in DMA2 was continuously scanned over sizes corresponding to diameter growth factors of 0.85–3.0, to ensure that no particles were missed. The particles were detected downstream DMA2 using a Condensation Particle Counter (CPC) (TSI model 3760A). In this case the dry sizes were selected cyclically to 35, 50, 75, 110, 165 and 265 nm, with two scans of 300 s per size (one up- and one down scan), making the time resolution of the measurements roughly one hour.

To validate the measurements, automatic $(\text{NH}_4)_2\text{SO}_4$ scans were carried out on a daily basis, as required by EUSAAR standards. These measurements consisted of one cycle, meaning that roughly 4% of the data consisted of salt scans. Dry scans were carried out on an irregular basis, with about 2–3 month intervals, and dry sizes were found stable within 2% of the nominal dry sizes. For further details regarding the H-TDMA system, see Nilsson et al. (2009).

Hygroscopic properties of the ambient aerosol in southern Sweden

E. O. Fors et al.

Title Page

Abstract

Introduction

Conclusions

References

Tables

Figures

⏪

⏩

◀

▶

Back

Close

Full Screen / Esc

Printer-friendly Version

Interactive Discussion



H-TDMA measurements started May 2008 and this paper covers the first 27 months of operation, ending in July 2010. During this time data coverage varied from month to month with an average of 66%, corresponding to roughly 200 000 scans. To facilitate the inversion, the TDMA-FIT software was used and continuous GF Probability Density Functions (GF-PDFs) were extracted from the data (Gysel et al., 2009). Criteria for a scan to be considered for inversion were that the average DMA2 RH in the scan should be between 88 and 92%, that the total number of counted particles should be more than 20, that DMA1 RH should be lower than 20% (to avoid an underestimated growth factor) and that the $(\text{NH}_4)_2\text{SO}_4$ scans confirmed the system functionality by a growth factor that was within corresponding values of $\pm 1.2\%$ RH of what can be expected according to growth factors predicted by the data from Tang and Munkelwitz (1994) and Potukuchi and Wexler (1995). To increase the comparability between different scans, the GF-PDFs were recalculated to 90% (Gysel et al., 2009).

2.2 DMPS

To measure the particle size distribution, a Differential Mobility Particle Sizer (DMPS) was used. The DMPS was constructed at Lund University and is a so called “twin-DMPS”, meaning that two parallel DMAs were used. The aerosol flow was dried and charged with an ^{85}Kr diffusion charger, whereafter the flow was split into two parts. One part of the flow was directed towards a Vienna-type nano DMA measuring diameters from 3.4 to 21.5 nm with a flow ratio of 3:21 l min^{-1} and the other part to a Vienna type long DMA, measuring between 21.5 and 857 nm with a flow ratio of 0.9:6.5 l min^{-1} .

By measuring the 21.5 nm concentration with both DMAs, an internal check was included in the measurements, as the two parallel systems should produce the same concentration, taking into account flows, CPC calibration curves and diffusion losses. The particles selected in the nano DMA and the long DMA were counted using two CPCs (TSI models 7610 and 3025 respectively). The system was operated in a step-wise manner over a total of 37 separated bins, with a time resolution of 10 min. For more details on the twin-DMPS system, see Kristensson et al. (2008).

2.3 CCN counter

The cloud nucleating properties of the aerosol was measured with a commercial CCNC (DMT model 100). The working principle of the instrument is to expose the aerosol to a fixed s value, and with an Optical Particle Counter (OPC) determine the number of activated particles. The aerosol continuously flows through the center part of a cylinder with wetted walls. Between the aerosol flow and the walls, there is a particle free sheath flow. By controlling the temperature of the walls and keeping them wet (i.e. assuring that the RH is 100% just outside the cylinder wall), the migration of heat and water vapour towards the middle of the cylinder and the s value can be controlled. The working principle relies on the fact that the water molecules diffuse towards the center faster than the heat added from the walls (which diffuses mainly via the heavier nitrogen and oxygen molecules), hence giving saturation ratios above 100%. The s values are altered in a cycle, and an activated CCN concentration as a function of s is determined.

In this case the values were 0.1, 0.2, 0.4, 0.7 and 1%, which covers basically all cloud formation s values found in the atmosphere (Twomey, 1959; Warner, 1968). The activated CCN concentration is given with a time resolution of one second, but since it takes time to equilibrate the system with respect to s , a measurement cycle takes ~30 m. More details on measurement uncertainties and principles of operation can be found in Rose et al. (2008).

2.4 The κ_R model and CCN closure

To validate measurement data, as well as test theoretical models and assumptions, so called “closure studies” can be performed. In principle, two or more independent measurements are linked together using relevant theoretical considerations, and in this way it is possible to indirectly evaluate if the instruments and models are consistent within errors of measurement. In this work, a CCN closure study has been carried out, comparing CCNC data with the predicted concentration of activated CCN(s) for each hour, using a combination of DMPS and H-TDMA data.

Hygroscopic properties of the ambient aerosol in southern Sweden

E. O. Fors et al.

Title Page

Abstract

Introduction

Conclusions

References

Tables

Figures

⏪

⏩

◀

▶

Back

Close

Full Screen / Esc

Printer-friendly Version

Interactive Discussion



The hygroscopic growth of an aerosol particle can be described by the Köhler equation (Köhler, 1936) according to

$$\rho_w(D_p) = \rho^0 a_w \exp\left(\frac{4M_w\sigma}{RT\rho_w D_w}\right) \quad (2)$$

where ρ_w is the water vapour partial pressure, ρ^0 the saturation water vapour pressure, a_w the water activity, M_w the molar weight of water, σ the surface tension the solution, R the universal gas constant, T the temperature, ρ_w the density of water, and D_w the wet diameter. In this work we describe the hygroscopicity of the particle with the parameter κ_R (Rissler et al., 2006, 2010), defined according to

$$GF = \sqrt[3]{1 + \kappa_R \cdot \chi_\phi \cdot \frac{M_w}{\rho_w} \cdot \frac{a_w}{1 - a_w}} \quad (3)$$

where κ_R is the number of soluble entities per dry volume unit and χ_ϕ a correction term introduced to account for non-ideal behaviour. The correction term is determined using a model salt, assuming that the non-ideality of the solution can be described by the non-ideality of the model salt at the same a_w . In this work, $(\text{NH}_4)_2\text{SO}_4$ was used as a model salt, since it is relatively abundant in the atmosphere. It can be noted that in sensitivity studies previously carried out, the choice of model salt did not prove to have a large effect on the predicted number of activated CCN(s_c) (Rissler et al., 2004). After calculating the κ_R from a specific growth factor and dry size, it is possible to find the critical supersaturation, s_c , corresponding to that particle using simplifications of Eq. (2) according to Seinfeld and Pandis (2006):

$$s_c = \sqrt{\frac{4A^3}{27C} \cdot \frac{1}{\kappa_R \cdot \chi_\phi \cdot D_p^3}} \quad (4)$$

where A and C are defined as

$$A = \frac{4M_w\sigma}{RT\rho_w} \quad \text{and} \quad C = \frac{M_w}{\rho_w} \quad (5)$$

Hygroscopic properties of the ambient aerosol in southern Sweden

E. O. Fors et al.

Title Page

Abstract

Introduction

Conclusions

References

Tables

Figures

⏪

⏩

◀

▶

Back

Close

Full Screen / Esc

Printer-friendly Version

Interactive Discussion



Hygroscopic properties of the ambient aerosol in southern Sweden

E. O. Fors et al.

[Title Page](#)[Abstract](#)[Introduction](#)[Conclusions](#)[References](#)[Tables](#)[Figures](#)[⏪](#)[⏩](#)[◀](#)[▶](#)[Back](#)[Close](#)[Full Screen / Esc](#)[Printer-friendly Version](#)[Interactive Discussion](#)

By combining DMPS and H-TDMA data, a distribution of corresponding s_c for the particle distribution at a given time can be obtained. By simply adding up all particles with $s_c < s_{CCNC}$, it is possible to make a prediction regarding the number concentration of activated CCN(s). For the CCN prediction, the GF-PDFs measured at 35, 50, 75, 110, 165 and 265 nm were linearly interpolated to create a hygroscopic growth factor surface function $f(D_p, GF)$. On this surface, each (D_p, GF) coordinate corresponds to a specific s_c value. For particles smaller than 35 nm, the 35 nm GF-PDF was assumed to be valid. In the same way, particles larger than 265 nm were assumed to have GF-PDFs identical to that of 265 nm particles.

The particles from one particular DMPS spectrum were then distributed over this surface function, after which the new surface function was integrated. In this case the GF integration steps were 0.05 and the D_p integration steps followed the DMPS data resolution. The data was then re-binned, this time as dN/ds_c , where N is the number concentration and s_c is the average s_c of that bin. As a final step, the dN/ds_c function was integrated up to any desired s ratio and can be compared to CCNC data, or used independently of the CCNC data, to create functions of the number of activated particles as a function of s .

If the salt model accurately describes the hygroscopic behavior of the aerosol and the instruments all were ideal, the measured CCNC(s) concentrations would be identical to the concentrations calculated from H-TDMA and DMPS data. However, considering a number of measurement uncertainties and assumptions in combination with particle non-idealities that are potentially not well represented by the modeling salt, certain imprecision can be expected. The linear interpolation of the GF-PDFs can be too coarse of an assumption, as can the extrapolation of the GF-PDFs corresponding to the smallest and largest particles measured by the H-TDMA. In addition to the resolution issues of the hygroscopicity measurements, the closure will underestimate the activated CCN(s) concentration if there are particles present that are larger than the DMPS can detect.

Hygroscopic properties of the ambient aerosol in southern Sweden

E. O. Fors et al.

Title Page

Abstract

Introduction

Conclusions

References

Tables

Figures

⏪

⏩

◀

▶

Back

Close

Full Screen / Esc

Printer-friendly Version

Interactive Discussion



Other possibilities are poor CPC calibration efficiency curves or a badly calibrated DMA flow which will affect the sizing – something that will likely affect low s values to a higher extent, as e.g. 0.2% s corresponds to particles is the centre of the size distribution to a higher extent than 1% s . As an example 100 nm particles with a GF of 1.6 activate at around 0.2% s , while 40 nm particles with a GF of 1.3 activate at 1% s .

Time resolution is another issue that introduces errors in the predicted concentration. In this aspect, the predicted concentration is limited by the H-TDMA data, which has a time resolution of 1 h, meaning that in a worst case scenario, there will be a difference of 15 min between the H-TDMA and the CCNC data. Fast changes in air masses can thus give large errors in the predicted concentrations. However, seen over a longer time period, no systematical error will be introduced by this effect, but rather a slightly decreased correlation coefficient.

2.5 Parameterisation of CCN(s) concentrations

To investigate how well the CCN concentrations could be described assuming a size dependent average GF from H-TDMA data, the log-normally fitted size distributions were integrated using a cumulative log-normal function according to Seinfeld and Pandis (2006):

$$N(D_p) = \frac{N}{2} + \frac{N}{2} \operatorname{erf} \left(\frac{\log(D_p / \bar{D}_{pg})}{\sqrt{2} \log(\sigma_g)} \right) \quad (6)$$

where

$$\operatorname{erf}(z) = \frac{2}{\sqrt{\pi}} \int_0^z e^{-\eta^2} d\eta \quad (7)$$

and \bar{D}_{pg} is the median diameter, σ_g is the geometric standard deviation and N is the number concentration. By calculating a critical dry diameter for a certain supersaturation ratio and then integrating the size distribution from that diameter and upwards for each size mode separately, it is possible to calculate CCN(s).

Hygroscopic properties of the ambient aerosol in southern Sweden

E. O. Fors et al.

Title Page

Abstract

Introduction

Conclusions

References

Tables

Figures

⏪

⏩

◀

▶

Back

Close

Full Screen / Esc

Printer-friendly Version

Interactive Discussion



In this work, CCN(*s*) concentration functions were produced, characteristic for the four seasons, and compared to CCNC data. The seasons were defined as follows: Spring (March–May), summer (June–August), autumn (September–November) and winter (December–February). In this case, two log-normal modes were used to fit averaged seasonal size distribution data, neglecting nucleation particle bursts. From the H-TDMA, four seasonal average sets of GF-PDFs were derived.

2.6 Petters' κ_p model

The parameter κ_p , first introduced by Petters and Kreidenweiss (2007), was used to describe the hygroscopicity of the aerosol. It was coincidentally named κ , as in Rissler et al. (2006), but with scaling for water density and molecular weight according to $\kappa_p = \kappa_R \cot \chi_\phi \frac{M_w}{V_w}$. It is an ideal model, meaning that the number of soluble entities is assumed to be independent of water activity. κ_p is defined according to

$$\frac{1}{a_w} = 1 + \kappa_p \frac{V_s}{V_w} \quad (8)$$

where V_w is the water volume and V_s is the soluble volume. For more details on comparison of the two κ models, see Rissler et al. (2010). κ_p is presently the most commonly used parameter to describe particle hygroscopicity, where values close to zero points to hydrophobic particles, and where values close to 1 are typical for hygroscopic aerosol, such as over marine areas.

3 Results

3.1 Data coverage

During the full 27 months of operation, the H-TDMA data coverage varied strongly, from 10% up to 95% on a monthly basis (Table 1). The data gaps were due to power failures

and software malfunctions as well as hardware issues. Seen over the whole period of operation the data coverage was on average 66%.

The data was quality checked with daily $(\text{NH}_4)_2\text{SO}_4$ scans. The results are illustrated in Fig. 1. The RH values have been recalculated to water activity, a_w , adjusting for the Kelvin effect, according to Eq. (2). In this way it becomes possible to visually display different dry sizes in the same plot. As can be seen, the measured values vary from day to day but the average values are close to the values derived from data from Potukuchi and Wexler (1995) and Tang and Munkelwitz (1994), and mostly within the $\pm 1.2\%$ which is the measurement uncertainty of the H-TDMA derived in Nilsson et al. (2009). There are a number of outliers, for which the cause of the deviation could not be determined. In these cases, data 12 h before and after that measurement point have been discarded. These cases accounted for $\sim 3\%$ of the scans.

3.2 Air mass origin during measurement period

Trajectories have been used to investigate the origin of the air masses arriving at Vavihill during the H-TDMA measurement period. This data has also been compared to trajectory data from the entire previous period when DMPS measurements have been performed at Vavihill (January 2001 to July 2010). The trajectory model Hysplit4 (Draxler and Hess, 1997) has been used to calculate the trajectories and meteorological data from the Centre of Environmental Predictions (NCEP), the FNL archive and GDAS (Global Data Assimilation System) archive have been used to calculate the trajectories. 72 h back trajectories originating at Vavihill 100 m above ground level have been used in the analysis and the centers of gravity of the trajectories have been calculated for each day. The azimuth angles and distances to the centers of gravity compared to Vavihill have then been calculated and the data divided according to season.

The results show that most air masses arrive to Vavihill from the west during all seasons and that they originate furthest from Vavihill during the winter and autumn, indicating fast moving air masses (Fig. 2). The H-TDMA measurement period May

Hygroscopic properties of the ambient aerosol in southern Sweden

E. O. Fors et al.

Title Page

Abstract

Introduction

Conclusions

References

Tables

Figures

⏪

⏩

◀

▶

Back

Close

Full Screen / Esc

Printer-friendly Version

Interactive Discussion



Hygroscopic properties of the ambient aerosol in southern Sweden

E. O. Fors et al.

Title Page

Abstract

Introduction

Conclusions

References

Tables

Figures

⏪

⏩

◀

▶

Back

Close

Full Screen / Esc

Printer-friendly Version

Interactive Discussion



2008 to May 2010 seem to be representative of the whole period for the spring, summer and autumn but not for the winter. The winters of 2008/2009 and 2000/2010 had fewer fast moving westerly air masses than the whole period between 2001 and 2010 and is instead dominated by slow moving air masses from the north and southeast. If the two winters are separated one can see that the winter 2008/2009 is more similar to the whole period with some fast moving westerly episodes but also a lot of northerly air masses. The winter 2009/2010 is instead dominated by slow-moving south-easterly and easterly air masses with barely any air masses arriving from the west; a result of a negative North Atlantic Oscillation. This winter was associated with below average temperatures in the region and long periods with high pressure cells situated over Eastern Europe.

3.3 Average GF-PDFs

Figure 3 illustrates GF-PDFs for all dry sizes, averaged over the full data set (see also Table 2). Some features of the averaged GF-PDFs seem to be size dependent. Firstly, the smaller particles have a larger fraction of the GF-PDF in the nearly hydrophobic and less hygroscopic part of the distribution. Secondly, the less hygroscopic mode tends to show lower GFs for larger particles. Thirdly, the more hygroscopic mode tends to show higher GFs for the larger particles.

The fact that the solubility of the more hygroscopic mode is increasing with size can be expected and has been found in previous studies (Swietlicki et al., 2008). It is most likely due to cloud processing of the particles. The difference in hygroscopicity between the more hygroscopic 35 and 50 nm particles is small, and part of the difference is due to the Kelvin effect. 165 and 265 nm are also similar, but from 75 to 110 nm there is a clear increase in hygroscopicity, as this is also the size at which the transition from the non-cloud processed Aitken mode to the cloud processed accumulation mode occurs.

It is important to be aware that the averaged functions can be somewhat misrepresentative. There are rarely any individual GF-PDFs with the shape of those in Fig. 3. The somewhat smeared appearance of the GF-PDFs is mostly an averaging effect. In

reality the individual GF-PDFs are commonly bi-modal with a clear separation of the two modes. For Aitken mode particles and below, a mono-modal distribution is more frequent than for the larger particles, and the GF-PDF is usually very dynamic, often changing several times per day. For the larger particles, the more hygroscopic mode is generally stable, while the less hygroscopic mode is more variable.

The reason for this difference is probably that the smallest particles are not as aged, and that fluctuations in meteorological conditions or air mass trajectories significantly alter particle properties. For the cloud processed particles, variations in the origin of the particles are not as important, since a large fraction of the particle consists of inorganic salts, originating from NH_3 , HNO_3 , H_2SO_4 and SO_2 which are dissolved as gasses in the aerosol liquid phase. SO_2 can subsequently be oxidized to H_2SO_4 , primarily by H_2O_2 and these substances recombine into inorganic salts composed of NH_4^+ , NO_3^- , HSO_4^- and SO_4^{2-} ions, with higher hygroscopic growth factors than organic substances.

3.4 Seasonal cycles

As previously stated, the hygroscopic properties of ambient particles are dynamic, both on shorter and longer time scale. The seasonal variability in the average growth factor is to large extent connected to the relative abundance of less and more hygroscopic particles. Figure 4 show monthly averaged GF-PDFs for all dry sizes. For 35 nm particles, it is clear that during wintertime, there is an increasing fraction of less hygroscopic particles. The growth factors of both the less and more hygroscopic modes seem to be stable over the annual cycle. There is some variation of the mode positions, but nothing that resembles an annual cycle. The 50 nm particles have a similar behavior to the 35 nm ones. They also have a clear bimodal distribution, where the relative abundance of less hygroscopic particles increases during winter, which in turn decreases the average growth factor. Also in this case it appears as if the two modes are relatively fixed in their respective growth factors.

Hygroscopic properties of the ambient aerosol in southern Sweden

E. O. Fors et al.

Title Page

Abstract

Introduction

Conclusions

References

Tables

Figures

⏪

⏩

◀

▶

Back

Close

Full Screen / Esc

Printer-friendly Version

Interactive Discussion



Hygroscopic properties of the ambient aerosol in southern Sweden

E. O. Fors et al.

[Title Page](#)[Abstract](#)[Introduction](#)[Conclusions](#)[References](#)[Tables](#)[Figures](#)[⏪](#)[⏩](#)[◀](#)[▶](#)[Back](#)[Close](#)[Full Screen / Esc](#)[Printer-friendly Version](#)[Interactive Discussion](#)

For the 75 nm particles, the distribution looks slightly different. The appearing and disappearing of less hygroscopic material during winter is still visible, if not as strong, but the more hygroscopic mode is more scattered. It appears as if the distribution is tri-modal at times, but this is only an effect of the averaging. Some of the particles found in the Aitken mode are capable of activating during a cloud formation process. When this happens, as described in Sect. 4.3, they increase their hygroscopicity and the GF of the more hygroscopic mode significantly increases.

For 110 nm particles there are also both cloud processed and non-cloud processed particles present, and the tri-modal appearance of the 75 nm particles is here even more pronounced. The less hygroscopic particles are now nearly hydrophobic, but still follow the seasonal pattern, being more frequent during winter. However, the relative frequency of these particles is considerably lower than for the smallest ones.

Unlike the 110 nm particles, there is only a weak hydrophobic mode appearing in the GF-PDF for the 165 and 265 nm particles, and it only appears during wintertime. As the particle size increases into the accumulation mode, the more hygroscopic mode increases in GF, and the nearly hydrophobic particles become even more hydrophobic. The reason for the appearance of particles with a GF around 1.3 in the summer for 165 and 265 nm diameter particles is unknown. While it might be an effect of air mass origin, it is out of scope of this paper to make a lengthy analysis of back trajectories.

To conclude, the GF-PDFs for all particle sizes measured have seasonal cycles, with a larger fraction of less hygroscopic or nearly hydrophobic particles present during winter. Tables 3 and 4 summarizes the seasonal trend, both with average GFs and κ_p values for each month according to Petters and Kreidenweis (2007) and with seasonal size dependent GF-PDFs.

Potential sources of the hydrophobic particles present during winter are not investigated in this study. However, it is likely that they originate from some form of combustion, such as residential biomass burning from wood stoves or oil burners, which are more intensively used during winter time and could produce soot particles in a wide size range. Parallel measurements of levoglucosan (Genberg et al., 2011), which is a

trace element for biomass burning (Simoneit et al., 1999) confirms this by showing a strong increase during winter.

On the other hand, measurements of organic and elemental carbon (OC and EC) on the site have shown that the soot concentration is relatively stable over the year, while the OC concentration increases during wintertime. During an intensive campaign in October 2008, Aerosol Mass Spectrometer (AMS) data was available from the measurement site, and in a hygroscopicity closure study it was concluded that the hydrophobic particles found at 265 nm are not entirely composed of soot, as there was a clear correlation between the appearing of completely hydrophobic material and the organic fraction measured by the AMS. It is possible that the hydrophobic particles consist of a combination of soot and HOA.

3.5 Diurnal cycles

Seen over shorter periods of time, the GF-PDFs of the growth factors are highly variably, especially for the smaller particle sizes. From one hour to the next, the GF-PDF can change, due to changes in meteorological conditions as e.g. mixing layer height, temperature fluctuations, or precipitation, as well as the origin of the air mass. These changes are seemingly random, but Fourier analysis revealed a diurnal cycle in the average growth factor. When averaging the volume weighted growth factors for the full data set, it turns out that the GF peaks at noon or early afternoon (Fig. 5a). This behavior is similar for all sizes, with the exception of 265 nm, which has its GF peak before noon. The reason for the different times of the maximum of GF for the 265 nm particles is not known.

The diurnal cycles found in this work are similar to those derived by e.g. Ehn et al. (2007) on freshly formed particles in boreal forest. Those particles also showed a strong diurnal cycle with GFs peaking in the afternoon for particles up to 50 nm, although the GFs of those particles was generally lower and the amplitude of the cycle slightly higher (for 35 nm the Finnish boreal particles had an average growth factor of 1.2 and an amplitude of 0.15 while our study found an average growth factor of 1.3 and

Hygroscopic properties of the ambient aerosol in southern Sweden

E. O. Fors et al.

Title Page

Abstract

Introduction

Conclusions

References

Tables

Figures

⏪

⏩

◀

▶

Back

Close

Full Screen / Esc

Printer-friendly Version

Interactive Discussion



an amplitude of 0.08). Other studies that have found the same type of diurnal trend with GF maxima in day time and minimum at night are Hämeri et al. (2001), Boy et al. (2004) and Petäjä et al. (2005). All these studies were conducted in boreal forest at the SMEAR II station in Hyytiälä, Finland.

5 In this study, most of the difference in GFs for 35, 50 and 75 nm can be explained by the Kelvin effect, and when recalculating the growth factors to κ_p values, the hygroscopicity of the three smallest particles were in principle identical, which can be interpreted as if they had the same chemical composition (Fig. 5b).

10 There are a number of possible reasons for the diurnal cycle in hygroscopicity. One is the diurnal evolution of the planetary boundary layer (PBL) as discussed in e.g. Rissler et al. (2006). In the morning, when the sun rises, the PBL increases in height and older particles are mixed down. In general, older particles are more hygroscopic, due to both an increased fraction of cloud processed particles, and to the fact that aging of the organic fraction in form of photolysis and oxidation increases its hygroscopicity
15 (Jimenez et al., 2009). For these reasons, the average aerosol GF-PDF will become more and more hygroscopic as the boundary layer increases in height. When the sun sets and the boundary layer collapses, local particle sources will have a bigger influence than they would have had during daytime, due to the low mixing height.

20 Nucleation mode particles have relatively short lifetimes. They either grow into the Aitken mode or coagulate with larger particles, which means that the diurnal cycle of the boundary layer will have less of an effect on the hygroscopicity of small particles compared to larger ones. Apart from these meteorological considerations, partitioning of semi-volatile species will follow the temperature which in turn follows the diurnal cycle. Primarily it is NO_3 (in the form of HNO_3) and semi-volatile organic species that
25 follow a diurnal cycle (Lanz et al., 2007; Raatikainen et al., 2010). HNO_3 dissolves in water and forms inorganic salts with relatively high GFs, which means that daytime evaporation will lead to a decrease in hygroscopicity. Evaporation of semi-volatile organics will on the other hand lead to an increased hygroscopicity, since generally the most volatile organics in the particle phase are also the ones with the lowest O:C ratio

Hygroscopic properties of the ambient aerosol in southern Sweden

E. O. Fors et al.

Title Page

Abstract

Introduction

Conclusions

References

Tables

Figures



Back

Close

Full Screen / Esc

Printer-friendly Version

Interactive Discussion

and hence the lowest hygroscopicity.

AMS measurements carried out at Vavihill during October 2008 confirm strong diurnal cycles in organic mass as well as NO_3 , but the NO_3 was only found in sizes larger than 80 nm with a strongly increasing volume fraction with increasing particle size. For particles below 80 nm, the aerosol mass consisted almost exclusively of organics and small amounts ($\sim 10\%$) of $(\text{NH}_4)_2\text{SO}_4$. With this in mind, it seems likely that the diurnal cycle seen for the 35 nm particles is at least partially driven by condensation and evaporation of organics.

Finally, diurnal cycles in the aerosol can be attributed to diurnal patterns of local sources. E.g. car emissions typically show peak values during rush hours. Massling et al. (2005) found a clear peak in nearly hydrophobic particles during morning rush hours at an urban measurement site. However, this pattern could not be found at the background station used for this study.

There was no clear annual pattern found in the amplitude of the diurnal GF cycle in any of the dry sizes. This would have been expected if variation in boundary layer height was the dominating effect, since the variation of the boundary layer height is strongly dependent on season. Instead we noted seemingly random monthly variations, most likely due to changes in meteorological conditions, and with the amplitude consistently higher for the smaller particles.

3.6 CCN closure

The CCN closure was carried out for the full data set for five different supersaturation ratios: 0.1, 0.2, 0.4, 0.7 and 1%. Figure 6 illustrates the scatter plot of 0.1% s and Fig. 7 illustrates the ratio of predicted and measured CCN concentrations for all s ratios. Table 5 presents the slope coefficients for all s closures. The salt model consistently predicted a lower CCN concentration than the CCNC. While the coefficient of determination was very similar for all cases (0.90 ± 0.01), the slope of the regression line varied from 0.74 for 0.2% supersaturation to 0.95 for 1% supersaturation and coefficients of determination, R^2 , between 0.91 and 0.94. The reason for this is not known,

Hygroscopic properties of the ambient aerosol in southern Sweden

E. O. Fors et al.

Title Page

Abstract

Introduction

Conclusions

References

Tables

Figures



Back

Close

Full Screen / Esc

Printer-friendly Version

Interactive Discussion



but a number of possible explanations can be hypothesized.

The CPCs used in the DMPS system have been calibrated using Ag particles and the calibration curves are used in the DMPS system in order not to underestimate the particle concentration. However, during an intercomparison workshop in March 2008 at the Institute for Atmospheric Research, IFT in Leipzig, the DMPS used in this closure measured 15% lower concentration than a CPC (TSI 3010) that was measuring total particle concentration simultaneously.

If this underprediction in number concentration is always present, it will lead to an underestimation of the CCN(s) concentration. However, when comparing the full DMPS size distribution to the measured CCN concentration at 1% s , which is the highest s value, the maximum CCN(s) values match the DMPS concentration well (Fig. 8), a fact that contradicts the counting efficiency of the CCN as the major problem in the closure. Of course there is also the possibility of the H-TDMA underestimating the particle hygroscopicity or the DMPS selecting the wrong sizes. Assuming that all instruments are functioning properly, it is the model that is incorrect. It has been shown before that the choice of modeling salt is not crucial to the model output (Rissler et al., 2004). There are numerous other static CCN models in the literature, and Rissler et al. (2004) found that they gave 6–10% difference in predicted CCN concentrations using seven different approaches for two different model aerosols.

The fact that the underprediction is stronger for low s_c ratios in this work can be explained by the fact that there are fewer particles in the sizes range which are close to activation at 1% (nucleation mode) than there is at 0.2% (Aitken or accumulation mode). An underestimation of the hygroscopicity would therefore have a larger impact at 0.2 than at 1% s . The uncertainty of the s measured by the CCNC also tends to increase for lower s (see e.g. Rose et al., 2008). To investigate the uncertainty introduced by error propagation from different measurement parameters, we used the precision of size distribution measurements from Wiedensohler et al. (2010) who compared a number of SMPS and DMPS systems in a laboratory environment and concluded that most systems measure a total particle concentration $\pm 10\%$ while the sizing of the particles

Hygroscopic properties of the ambient aerosol in southern Sweden

E. O. Fors et al.

Title Page

Abstract

Introduction

Conclusions

References

Tables

Figures



Back

Close

Full Screen / Esc

Printer-friendly Version

Interactive Discussion

can be expected to be accurate with $\pm 3.5\%$. In addition to this, the H-TDMA is estimated to measure growth factors within 3% precision in GF due to uncertainties in the RH measurement.

For simplification, we used the average GF-PDFs and the average size distribution for the entire measurement period and calculated the relative change in predicted CCN concentrations for 0.1, 0.2, 0.4, 0.7 and 1% s . The shape of the size distribution makes the uncertainty very varying (see Table 6). For all s except 0.2% s , the super positioned measurement uncertainties can hypothetically explain the difference in measured and predicted CCN concentration. For 0.2% however, there is still a difference of 7%, even after introducing all measurement uncertainty. An additional uncertainty in the CCNC could possibly explain the last percent, but it seems unlikely that all measurement errors would point in the same direction with respect to the closure.

Another measurement artifact that might play a role is that particles may not have reached their equilibrium with respect to the surrounding water vapour. Firstly, the aerosol must be completely dry when it enters DMA1. If it is not, and it keeps shrinking until it reaches the humidifier, the GF will be underestimated. In the same manner, if it does not reach the humidified diameter before entering DMA2 (the humid residence time is ~ 1 s), the GF will be further underestimated. These two effects will both lead to an underestimation of the CCN concentration, especially at s values corresponding to diameters in the middle of the size distribution. Finally, drying of the aerosol in the DMPS can play a role. If the particles are not completely dried out, the sizes will be overestimated, which will lead to an overestimation of the CCN concentration.

In addition to measurement uncertainties, aerosol properties can play a role. It is possible that compounds as K_2SO_4 which have a limited solubility will lead to an overestimation of the s_c or that there are particles larger present than what is measured by the DMPS, something that would play a larger role for low s values. Another possibility is that the particles contain surface active compounds such as HULIS, which has been proposed to originate from polymerization in the aqueous phase, formed through ageing of particles (Graber and Rudich, 2006). No seasonal or diurnal cycle was found

Hygroscopic properties of the ambient aerosol in southern Sweden

E. O. Fors et al.

Title Page

Abstract

Introduction

Conclusions

References

Tables

Figures



Back

Close

Full Screen / Esc

Printer-friendly Version

Interactive Discussion



in the ratio of modeled to measured CCN concentrations. Distinct periods of different ratios were found, rather than the continuous change that one might expect from e.g. seasonal sources such as biogenic SOA or combustion particles from heating.

This underprediction of CCN concentrations based on subsaturated measurements has to our knowledge not been found in previous CCN closure studies, which indicates that it is in fact a measurement effect rather than an aerosol effect. Moreover, previously published CCN closure studies have tended to overestimate the number of CCN (Kammermann et al., 2010b; McFiggans et al., 2006).

3.7 CCN parameterization

Finally, a parameterization of the activated CCN(*s*) concentration was carried out, based on seasonal averages and compared to seasonal CCNC data (Table 7). Average DMPS size distribution spectrums for the four seasons were derived (Fig. 9), as well as seasonal average GF-PDFs for the different dry sizes. A modal fit routine was then applied to describe the average distribution with three log-normal modes (Hussein et al., 2005) (Table 8). The mode with smallest particle diameter, if GMD was smaller than 20 nm, was then excluded for each season. The reason for this was to avoid bias from frequently occurring nucleation bursts when comparing the fraction of activated particles for a specific *s*. For more details on the number size distribution of Vavihill, see Kristensson et al. (2008).

The averaged and mode-fitted size distributions were used to calculate CCN(*s*) for different seasons applying two different approaches: (1) using the full external mixture of the aerosol, and (2) Calculating size dependent GFs from 3rd moment averaged GF-PDFs, and linearly interpolating to the geometric mean values of the fitted log-normal distributions. From this data the cumulative log-normal distribution described in Sect. 3.5 was used to calculate CCN(*s*) functions. It was found that the second approach produced CCN(*s*) functions very similar to taking the full GF-PDF into account (Fig. 10a–d).

For 1% *s*, CCN concentrations were highest during summer and spring, followed by

Hygroscopic properties of the ambient aerosol in southern Sweden

E. O. Fors et al.

Title Page

Abstract

Introduction

Conclusions

References

Tables

Figures



Back

Close

Full Screen / Esc

Printer-friendly Version

Interactive Discussion



autumn, and the lowest concentration was found during winter. This can partially be attributed to the concentration of Aitken mode particles, which largely follow the same order, and partially by the hygroscopic growth, which was found to be higher during summertime. For lower s ratios, winter showed the highest CCN concentration, due to a larger accumulation mode, followed by summer and spring and finally autumn, which presented the lowest CCN concentration.

Considering the high STD values of the seasonally averaged CCN concentrations, it can be concluded that the CCN(s) functions derived from averaged DMPS and H-TDMA data well describe the CCN concentrations for different seasons, and that the assumption of an internally mixed aerosol with respect to hygroscopic properties in this case was adequate for describing the CCN(s) concentration of a European continental background aerosol.

4 Summary and conclusions

Hygroscopic properties of the aerosol at the background EUSAAR supersite Vavihill has been measured over a period of 27 months. H-TDMA data has been analysed with respect to temporal variability with focus both on seasonal and diurnal cycles. A CCN closure study has been carried out and parameterisations of CCN(s) concentrations for different seasons have been produced.

In general, the aerosol was often externally mixed with respect to hygroscopic growth, with GFs of both the less hygroscopic and more hygroscopic modes varying in time. Smaller particles were found to have a higher fraction of less hygroscopic particles. There is also a trend of increasing separation between the two hygroscopic modes with increasing size. The high GFs of the larger particles can most likely be attributed to a combination of chemical ageing and cloud processing, where soluble gases have added inorganic ions to the particle after the cloud drop dry out.

Hygroscopic properties of the ambient aerosol in southern Sweden

E. O. Fors et al.

Title Page

Abstract

Introduction

Conclusions

References

Tables

Figures

⏪

⏩

◀

▶

Back

Close

Full Screen / Esc

Printer-friendly Version

Interactive Discussion

Hygroscopic properties of the ambient aerosol in southern Sweden

E. O. Fors et al.

Title Page

Abstract

Introduction

Conclusions

References

Tables

Figures

⏪

⏩

◀

▶

Back

Close

Full Screen / Esc

Printer-friendly Version

Interactive Discussion



In general, the GF of the modes in the averaged GF-PDFs were stable during the year, but the relative abundance of the modes changed with season. This seasonal cycle of the GF-PDFs was found to be most pronounced for the smallest particles. The mode of less hygroscopic particles increased in relative abundance during winter time. These less hygroscopic particles were more frequent during winter also for the larger particles, though the trend weakened with increasing size.

On a diurnal basis, all particles except 265 nm were found to have a higher growth factor during day-time than during night-time.

The CCN closure slightly underpredicted the number of activated CCN(*s*), from nearly 25% at 0.2% *s* to 5% at 1% *s*. The reason for this is unknown, though it is most likely connected to a combination of different measurement and modelling errors.

Finally it was concluded that seasonal averaged data from the DMPS and H-TDMA measurements well described the CCN concentrations from the DMT CCNC. It was also found possible to simplify the aerosol description by assuming a bimodal size distribution with an average modal GF without significantly increasing the difference between measured and modelled CCN concentrations.

The results presented in this work may serve as input to models which desire to incorporate the hygroscopic properties of the atmospheric aerosol. However, the results also raise many unanswered questions regarding the mechanisms that control the hygroscopic properties of the ambient aerosol, and even though we have speculated around possible explanations for the different phenomena, deeper understanding of the processes involved will require detailed studies of the respective mechanisms.

Acknowledgements. This work was carried out with the support of the FP6 European Commission project European Supersites for Atmospheric Aerosol Research, EUSAAR, contract No. RII3-CT-2006-026140, the European Integrated Project on Aerosol, Cloud, Climate and Air Quality Interactions, EUCAARI, contract number 036833-2, the Strategic Research Program MERGE: Modelling the Regional and Global Earth System, and Lund Centre for studies of Carbon Cycle and Climate Interaction – LUCCI. The DMPS measurements at Vavihill were supported by the Swedish Environmental Protection Agency within the Swedish Environmental Monitoring Program. The support by the Swedish Research Council for Environment, Agricul-

tural Sciences and Spatial Planning (Formas) through project No. 2009-615 and 2008-1467 is also gratefully acknowledged. Finally Joonas Merikanto is acknowledged for valuable discussions on how to best incorporate hygroscopic data in global models and Martin Gysel is acknowledged for the use of the TDMA inversion algorithm TDMAinv.

5 References

- Boy, M., Petäjä, T., Dal Maso, M., Rannik, Ü., Rinne, J., Aalto, P., Laaksonen, A., Vaattovaara, P., Joutsensaari, J., Hoffmann, T., Warnke, J., Apostolaki, M., Stephanou, E. G., Tsapakis, M., Kouvarakis, A., Pio, C., Carvalho, A., Römpf, A., Moortgat, G., Spirig, C., Guenther, A., Greenberg, J., Ciccioli, P., and Kulmala, M.: Overview of the field measurement campaign in Hyytiälä, August 2001 in the framework of the EU project OSOA, *Atmos. Chem. Phys.*, 4, 657–678, doi:10.5194/acp-4-657-2004, 2004.
- Draxler, R. and Hess, G.: Description of the HYSPLIT_4 modeling system, NOAA Technical Memorandum ERL ARL-224, 24, 1997.
- Duplissy, J., Gysel, M., Sjogren, S., Meyer, N., Good, N., Kammermann, L., Michaud, V., Weigel, R., Martins dos Santos, S., Gruening, C., Villani, P., Laj, P., Sellegri, K., Metzger, A., McFiggans, G. B., Wehrle, G., Richter, R., Dommen, J., Ristovski, Z., Baltensperger, U., and Weingartner, E.: Intercomparison study of six HTDMAs: results and recommendations, *Atmos. Meas. Tech.*, 2, 363–378, doi:10.5194/amt-2-363-2009, 2009.
- Dusek, U., Frank, G., Hildebrandt, L., Curtius, J., Schneider, J., Walter, S., Chand, D., Drewnick, F., Hings, S., and Jung, D.: Size matters more than chemistry for cloud-nucleating ability of aerosol particles, *Science*, 312, 1375, doi:10.1126/science.1125261, 2006.
- Ehn, M., Petäjä, T., Aufmhoff, H., Aalto, P., Hämeri, K., Arnold, F., Laaksonen, A., and Kulmala, M.: Hygroscopic properties of ultrafine aerosol particles in the boreal forest: diurnal variation, solubility and the influence of sulfuric acid, *Atmos. Chem. Phys.*, 7, 211–222, doi:10.5194/acp-7-211-2007, 2007.
- Fierz-Schmidhauser, R., Zieger, P., Wehrle, G., Jefferson, A., Ogren, J. A., Baltensperger, U., and Weingartner, E.: Measurement of relative humidity dependent light scattering of aerosols, *Atmos. Meas. Tech.*, 3, 39–50, doi:10.5194/amt-3-39-2010, 2010.
- Genberg, J., Hyder, M., Stenström, K., Fors, E. O., Sporre, M., and Swietlicki, E.: Source Apportionment of Carbonaceous Aerosol in Southern Sweden, in preparation, 2011.

Hygroscopic properties of the ambient aerosol in southern Sweden

E. O. Fors et al.

Title Page

Abstract

Introduction

Conclusions

References

Tables

Figures

⏪

⏩

◀

▶

Back

Close

Full Screen / Esc

Printer-friendly Version

Interactive Discussion



Hygroscopic properties of the ambient aerosol in southern Sweden

E. O. Fors et al.

[Title Page](#)[Abstract](#)[Introduction](#)[Conclusions](#)[References](#)[Tables](#)[Figures](#)[⏪](#)[⏩](#)[◀](#)[▶](#)[Back](#)[Close](#)[Full Screen / Esc](#)[Printer-friendly Version](#)[Interactive Discussion](#)

- Graber, E. R. and Rudich, Y.: Atmospheric HULIS: How humic-like are they? A comprehensive and critical review, *Atmos. Chem. Phys.*, 6, 729–753, doi:10.5194/acp-6-729-2006, 2006.
- Gysel, M., McFiggans, G., and Coe, H.: Inversion of tandem differential mobility analyser (TDMA) measurements, *J. Aerosol Sc.*, 40, 134–151, 2009.
- 5 Hussein, T., Dal Maso, M., Petaja, T., Koponen, I. K., Paatero, P., Aalto, P. P., Hameri, K., and Kulmala, M.: Evaluation of an automatic algorithm for fitting the particle number size distributions, *Boreal Environ. Res.*, 10, 337–355, 2005.
- Hämeri, K., Väkevä, M., Aalto, P., Kulmala, M., Swietlicki, E., Zhou, J., Seidl, W., Becker, E., and O’dowd, C.: Hygroscopic and CCN properties of aerosol particles in boreal forests, *Tellus B*, 10
53, 359–379, 2001.
- Jimenez, J., Canagaratna, M., Donahue, N., Prevot, A., Zhang, Q., Kroll, J., DeCarlo, P., Allan, J., Coe, H., and Ng, N.: Evolution of organic aerosols in the atmosphere, *Science*, 326, 1525, doi:10.1126/science.1180353, 2009.
- Kammermann, L., Gysel, M., Weingartner, E., and Baltensperger, U.: 13-month climatology of the aerosol hygroscopicity at the free tropospheric site Jungfraujoch (3580 m a.s.l.), *Atmos. Chem. Phys.*, 10, 10717–10732, doi:10.5194/acp-10-10717-2010, 2010a.
- 15 Kammermann, L., Gysel, M., Weingartner, E., Herich, H., Cziczo, D. J., Holst, T., Svenningson, B., Arneth, A., and Baltensperger, U.: Subarctic atmospheric aerosol composition: 3. Measured and modeled properties of cloud condensation nuclei, *J. Geophys. Res.-Atmos.*, 20
115, D04202, doi:10.1029/2009jd012447, 2010b.
- Kristensson, A. and Dal, M.: Characterization of new particle formation events at a background site in Southern Sweden: relation to air mass history, *Tellus B*, 60, 330–344, 2008.
- Kristensson, A., Dal Maso, M., Swietlicki, E., Hussein, T., Zhou, J., Kerminen, V. M., and Kulmala, M.: Characterization of new particle formation events at a background site in Southern Sweden: relation to air mass history, *Tellus B*, 60, 330–344, doi:10.1111/j.1600-0889.2008.00345.x, 2008.
- 25 Köhler, H.: The nucleus in and the growth of hygroscopic droplets, *Trans. Faraday Soc.*, 32, 1152–1161, 1936.
- Lanz, V. A., Alfarra, M. R., Baltensperger, U., Buchmann, B., Hueglin, C., and Prévôt, A. S. H.: Source apportionment of submicron organic aerosols at an urban site by factor analytical modelling of aerosol mass spectra, *Atmos. Chem. Phys.*, 7, 1503–1522, doi:10.5194/acp-7-1503-2007, 2007.
- 30 Massling, A., Stock, M., and Wiedensohler, A.: Diurnal, weekly, and seasonal variation of

Hygroscopic properties of the ambient aerosol in southern Sweden

E. O. Fors et al.

[Title Page](#)[Abstract](#)[Introduction](#)[Conclusions](#)[References](#)[Tables](#)[Figures](#)[⏪](#)[⏩](#)[◀](#)[▶](#)[Back](#)[Close](#)[Full Screen / Esc](#)[Printer-friendly Version](#)[Interactive Discussion](#)

hygroscopic properties of submicrometer urban aerosol particles, *Atmos. Environ.*, 39, 3911–3922, 2005.

McFiggans, G., Artaxo, P., Baltensperger, U., Coe, H., Facchini, M. C., Feingold, G., Fuzzi, S., Gysel, M., Laaksonen, A., Lohmann, U., Mentel, T. F., Murphy, D. M., O'Dowd, C. D., Snider, J. R., and Weingartner, E.: The effect of physical and chemical aerosol properties on warm cloud droplet activation, *Atmos. Chem. Phys.*, 6, 2593–2649, doi:10.5194/acp-6-2593-2006, 2006.

Nilsson, E., Swietlicki, E., Sjogren, S., Löndahl, J., Nyman, M., and Svenningsson, B.: Development of an H-TDMA for long-term unattended measurement of the hygroscopic properties of atmospheric aerosol particles, *Atmos. Meas. Tech.*, 2, 313–318, doi:10.5194/amt-2-313-2009, 2009.

Petäjä, T., Kerminen, V.-M., Hämeri, K., Vaattovaara, P., Joutsensaari, J., Junkermann, W., Laaksonen, A., and Kulmala, M.: Effects of SO₂ oxidation on ambient aerosol growth in water and ethanol vapours, *Atmos. Chem. Phys.*, 5, 767–779, doi:10.5194/acp-5-767-2005, 2005.

Petters, M. D. and Kreidenweis, S. M.: A single parameter representation of hygroscopic growth and cloud condensation nucleus activity, *Atmos. Chem. Phys.*, 7, 1961–1971, doi:10.5194/acp-7-1961-2007, 2007.

Potukuchi, S. and Wexler, A. S.: Identifying solid-aqueous phase transitions in atmospheric aerosols—I. Neutral-acidity solutions, *Atmos. Environ.*, 29, 1663–1676, 1995.

Raatikainen, T., Vaattovaara, P., Tiitta, P., Miettinen, P., Rautiainen, J., Ehn, M., Kulmala, M., Laaksonen, A., and Worsnop, D. R.: Physicochemical properties and origin of organic groups detected in boreal forest using an aerosol mass spectrometer, *Atmos. Chem. Phys.*, 10, 2063–2077, doi:10.5194/acp-10-2063-2010, 2010.

Rader, D. and McMurry, P.: Application of the tandem differential mobility analyzer to studies of droplet growth or evaporation, *J. Aerosol Sci.*, 17, 771–787, 1986.

Rissler, J., Swietlicki, E., Zhou, J., Roberts, G., Andreae, M. O., Gatti, L. V., and Artaxo, P.: Physical properties of the sub-micrometer aerosol over the Amazon rain forest during the wet-to-dry season transition – comparison of modeled and measured CCN concentrations, *Atmos. Chem. Phys.*, 4, 2119–2143, doi:10.5194/acp-4-2119-2004, 2004.

Rissler, J., Vestin, A., Swietlicki, E., Fisch, G., Zhou, J., Artaxo, P., and Andreae, M. O.: Size distribution and hygroscopic properties of aerosol particles from dry-season biomass burning in Amazonia, *Atmos. Chem. Phys.*, 6, 471–491, doi:10.5194/acp-6-471-2006, 2006.

Hygroscopic properties of the ambient aerosol in southern Sweden

E. O. Fors et al.

[Title Page](#)[Abstract](#)[Introduction](#)[Conclusions](#)[References](#)[Tables](#)[Figures](#)[⏪](#)[⏩](#)[◀](#)[▶](#)[Back](#)[Close](#)[Full Screen / Esc](#)[Printer-friendly Version](#)[Interactive Discussion](#)

- Rissler, J., Svenningsson, B., Fors, E. O., Bilde, M., and Swietlicki, E.: An evaluation and comparison of cloud condensation nucleus activity models: Predicting particle critical saturation from growth at subsaturation, *J. Geophys. Res.*, 115, D22208, doi:10.1029/2010JD014391, 2010.
- 5 Rose, D., Gunthe, S. S., Mikhailov, E., Frank, G. P., Dusek, U., Andreae, M. O., and Pöschl, U.: Calibration and measurement uncertainties of a continuous-flow cloud condensation nuclei counter (DMT-CCNC): CCN activation of ammonium sulfate and sodium chloride aerosol particles in theory and experiment, *Atmos. Chem. Phys.*, 8, 1153–1179, doi:10.5194/acp-8-1153-2008, 2008.
- 10 Rosenfeld, D.: TRMM observed first direct evidence of smoke from forest fires inhibiting rainfall, *Geophys. Res. Lett.*, 26, 3105–3108, 1999.
- Rosenfeld, D.: Suppression of rain and snow by urban and industrial air pollution, *Science*, 287, 1793, doi:10.1126/science.287.5459.1793, 2000.
- Seinfeld, J. H. and Pandis, S. N.: *Atmospheric Chemistry and Physics – From Air Pollution to Climate Change*, 2nd edition, Wiley Interscience, 2006.
- 15 Sekigawa, K.: Estimation of the volume fraction of water soluble material in submicron aerosols in the atmosphere, *Journal of the Meteorological Society of Japan*, 61, 359–367, 1983.
- Simoneit, B. R. T., Schauer, J. J., Nolte, C., Oros, D. R., Elias, V. O., Fraser, M., Rogge, W., and Cass, G. R.: Levoglucosan, a tracer for cellulose in biomass burning and atmospheric particles, *Atmos. Environ.*, 33, 173–182, 1999.
- 20 Solomon, S.: *Climate change 2007: the physical science basis*, Cambridge University Press Cambridge, 2007.
- Swietlicki, E., HANSSON, H. C., Hämeri, K., Svenningsson, B., Massling, A., McFiggans, G., McMurry, P., Petäjä, T., Tunved, P., and Gysel, M.: Hygroscopic properties of submicrometer atmospheric aerosol particles measured with H TDMA instruments in various environments – A review, *Tellus B*, 60, 432–469, 2008.
- 25 Tang, I. N. and Munkelwitz, H. R.: Water activities, densities and refractive-indexes of aqueous sulfates and sodium-nitrate droplets of atmospheric importance, *J. Geophys. Res.*, 99, 18801–18808, doi:10.1029/94JD01345, 1994.
- 30 Twomey, S.: The nuclei of natural cloud formation part II: The supersaturation in natural clouds and the variation of cloud droplet concentration, *PureApplied Geophys.*, 43, 243–249, 1959.
- Warner, J.: The supersaturation in natural clouds, *J. Rech. Atmos*, 3, 233–237, 1968.
- Wiedensohler, A., Birmili, W., Nowak, A., Sonntag, A., Weinhold, K., Merkel, M., Wehner, B.,

5 Tuch, T., Pfeifer, S., Fiebig, M., Fjåraa, A. M., Asmi, E., Sellegri, K., Depuy, R., Venzac, H., Villani, P., Laj, P., Aalto, P., Ogren, J. A., Swietlicki, E., Roldin, P., Williams, P., Quincey, P., Hüglin, C., Fierz-Schmidhauser, R., Gysel, M., Weingartner, E., Riccobono, F., Santos, S., Grüning, C., Faloon, K., Beddows, D., Harrison, R. M., Monahan, C., Jennings, S. G., O'Dowd, C. D., Marinoni, A., Horn, H.-G., Keck, L., Jiang, J., Scheckman, J., McMurry, P. H., Deng, Z., Zhao, C. S., Moerman, M., Henzing, B., and de Leeuw, G.: Particle mobility size spectrometers: harmonization of technical standards and data structure to facilitate high quality long-term observations of atmospheric particle number size distributions, Atmos. Meas. Tech. Discuss., 3, 5521–5587, doi:10.5194/amtd-3-5521-2010, 2010.

ACPD

11, 6601–6650, 2011

Hygroscopic properties of the ambient aerosol in southern Sweden

E. O. Fors et al.

[Title Page](#)[Abstract](#)[Introduction](#)[Conclusions](#)[References](#)[Tables](#)[Figures](#)[⏪](#)[⏩](#)[◀](#)[▶](#)[Back](#)[Close](#)[Full Screen / Esc](#)[Printer-friendly Version](#)[Interactive Discussion](#)

Hygroscopic properties of the ambient aerosol in southern Sweden

E. O. Fors et al.

Title Page

Abstract

Introduction

Conclusions

References

Tables

Figures

⏪

⏩

◀

▶

Back

Close

Full Screen / Esc

Printer-friendly Version

Interactive Discussion



Table 2. Average GF-PDFs with standard deviations for different dry sizes during the entire measurement period.

GF	35 nm	50 nm	75 nm	110 nm	165 nm	265 nm
0.9	0.06±0.28	0.02±0.14	0.02±0.19	0.02±0.17	0.02±0.18	0.14±0.48
1	0.68±1	0.55±0.8	0.67±0.84	0.75±0.89	0.59±0.74	0.58±0.88
1.1	1.6±1.8	1.26±1.54	1.14±1.21	0.81±0.89	0.6±0.7	0.64±0.79
1.2	1.41±1.57	1.32±1.48	1.12±1.33	0.78±1.18	0.5±0.96	0.28±0.6
1.3	2.42±1.79	2.28±1.59	1.92±1.28	1.37±1.12	0.97±1.1	0.68±1
1.4	2.46±2	2.82±1.88	2.21±1.57	1.51±1.43	1.12±1.25	0.82±1.08
1.5	0.93±1.43	1.4±1.65	2.12±1.69	2.5±1.8	2.1±1.89	1.37±1.67
1.6	0.22±0.81	0.25±0.83	0.64±1.14	1.82±2	2.85±2.29	2.83±2.31
1.7	0.08±0.5	0.07±0.48	0.11±0.57	0.3±0.86	1.05±1.75	2.1±2.35
1.8	0.03±0.3	0.01±0.1	0.03±0.28	0.04±0.35	0.1±0.44	0.37±0.97
1.9	0.03±0.24	0±0.05	0.01±0.06	0.01±0.11	0.02±0.19	0.09±0.45
2	0.01±0.1	0±0.04	0±0.03	0±0.06	0.01±0.11	0.11±0.43
2.1	0.01±0.12	0±0.04	0±0.05	0.02±0.15	0.02±0.17	0±0
2.2	0.02±0.1	0±0.06	0±0.04	0.01±0.07	0±0.08	0±0.01
2.3	0±0.04	0±0.02	0±0.04	0±0.05	0±0.06	0±0
2.4	0±0.03	0±0.02	0±0.04	0±0.07	0±0.06	0±0
2.5	0.03±0.16	0.01±0.08	0.01±0.09	0±0.28	0.05±0.3	0±0

Table 3. Monthly GFs and κ_P values averaged over 27 months.

Growth factor mean												
	Jan	Feb	Mar	Apr	May	Jun	Jul	Aug	Sep	Oct	Nov	Dec
35 nm	1.27	1.30	1.32	1.33	1.32	1.31	1.31	1.30	1.30	1.27	1.27	1.27
50 nm	1.30	1.33	1.34	1.36	1.35	1.34	1.34	1.33	1.31	1.29	1.29	1.29
75 nm	1.35	1.36	1.37	1.39	1.39	1.37	1.37	1.35	1.33	1.31	1.31	1.30
110 nm	1.41	1.45	1.44	1.42	1.45	1.42	1.41	1.40	1.37	1.37	1.38	1.37
165 nm	1.47	1.46	1.51	1.48	1.52	1.47	1.47	1.47	1.44	1.45	1.46	1.44
265 nm	1.49	1.44	1.58	1.54	1.57	1.51	1.50	1.50	1.48	1.50	1.52	1.52
Growth factor median												
35 nm	1.27	1.31	1.32	1.33	1.33	1.30	1.31	1.31	1.30	1.28	1.28	1.28
50 nm	1.31	1.34	1.35	1.36	1.35	1.33	1.34	1.34	1.32	1.31	1.30	1.30
75 nm	1.35	1.37	1.37	1.39	1.39	1.36	1.36	1.36	1.33	1.32	1.31	1.31
110 nm	1.42	1.46	1.43	1.43	1.46	1.41	1.41	1.41	1.38	1.38	1.38	1.37
165 nm	1.49	1.47	1.51	1.49	1.53	1.45	1.47	1.47	1.44	1.46	1.46	1.44
265 nm	1.51	1.45	1.59	1.54	1.58	1.50	1.52	1.50	1.48	1.51	1.53	1.52
Growth factor std												
35 nm	0.10	0.08	0.08	0.09	0.10	0.11	0.09	0.09	0.10	0.09	0.08	0.09
50 nm	0.08	0.07	0.07	0.09	0.10	0.10	0.09	0.08	0.09	0.08	0.07	0.08
75 nm	0.07	0.06	0.07	0.09	0.10	0.10	0.09	0.08	0.08	0.08	0.06	0.06
110 nm	0.09	0.12	0.08	0.08	0.11	0.11	0.10	0.09	0.08	0.08	0.07	0.07
165 nm	0.10	0.11	0.07	0.09	0.11	0.12	0.12	0.10	0.09	0.09	0.08	0.08
265 nm	0.12	0.11	0.08	0.10	0.10	0.11	0.11	0.09	0.10	0.11	0.09	0.09

Hygroscopic properties of the ambient aerosol in southern Sweden

E. O. Fors et al.

Title Page

Abstract

Introduction

Conclusions

References

Tables

Figures

⏪

⏩

◀

▶

Back

Close

Full Screen / Esc

Printer-friendly Version

Interactive Discussion

Hygroscopic properties of the ambient aerosol in southern Sweden

E. O. Fors et al.

Title Page

Abstract

Introduction

Conclusions

References

Tables

Figures

⏪

⏩

◀

▶

Back

Close

Full Screen / Esc

Printer-friendly Version

Interactive Discussion



Table 3. Continued.

Growth factor mean												
	Jan	Feb	Mar	Apr	May	Jun	Jul	Aug	Sep	Oct	Nov	Dec
κ_p mean												
35 nm	0.16	0.18	0.20	0.21	0.20	0.19	0.19	0.19	0.18	0.16	0.16	0.16
50 nm	0.17	0.19	0.20	0.21	0.20	0.20	0.20	0.19	0.18	0.16	0.16	0.16
75 nm	0.19	0.20	0.21	0.22	0.22	0.21	0.20	0.19	0.17	0.17	0.16	0.16
110 nm	0.22	0.26	0.24	0.23	0.26	0.24	0.23	0.22	0.20	0.20	0.20	0.19
165 nm	0.26	0.25	0.29	0.27	0.30	0.26	0.26	0.26	0.24	0.24	0.25	0.24
265 nm	0.28	0.24	0.34	0.31	0.34	0.29	0.28	0.28	0.26	0.28	0.29	0.29
κ_p median												
35 nm	0.16	0.19	0.20	0.20	0.20	0.18	0.19	0.19	0.18	0.17	0.17	0.17
50 nm	0.17	0.19	0.20	0.21	0.20	0.19	0.19	0.19	0.18	0.17	0.17	0.17
75 nm	0.19	0.20	0.20	0.21	0.21	0.20	0.20	0.19	0.18	0.17	0.16	0.16
110 nm	0.22	0.26	0.24	0.23	0.26	0.22	0.22	0.22	0.20	0.20	0.20	0.19
165 nm	0.27	0.26	0.29	0.27	0.30	0.24	0.26	0.26	0.24	0.25	0.25	0.24
265 nm	0.29	0.24	0.35	0.31	0.34	0.27	0.29	0.28	0.26	0.28	0.30	0.29
κ_p std												
35 nm	0.07	0.06	0.06	0.07	0.07	0.08	0.06	0.06	0.07	0.06	0.05	0.06
50 nm	0.06	0.05	0.05	0.06	0.07	0.07	0.06	0.06	0.06	0.05	0.05	0.05
75 nm	0.05	0.04	0.05	0.06	0.07	0.07	0.06	0.05	0.05	0.05	0.04	0.04
110 nm	0.06	0.07	0.06	0.06	0.08	0.08	0.07	0.06	0.05	0.05	0.05	0.05
165 nm	0.07	0.06	0.06	0.07	0.09	0.09	0.08	0.07	0.06	0.06	0.06	0.06
265 nm	0.08	0.08	0.07	0.08	0.08	0.09	0.09	0.07	0.07	0.09	0.07	0.07

Table 4. Seasonal averaged GF-PDFs with corresponding standard deviations.

GF	Spring						Summer					
	35 nm	50 nm	75 nm	110 nm	165 nm	265 nm	35 nm	50 nm	75 nm	110 nm	165 nm	265 nm
0.9	0.04±0.13	0.02±0.09	0.03±0.09	0.02±0.1	0.02±0.14	0.08±0.28	0.05±0.38	0.01±0.14	0.01±0.07	0.02±0.14	0.02±0.15	0.07±0.29
1	0.49±0.74	0.4±0.63	0.48±0.69	0.53±0.7	0.44±0.61	0.37±0.56	0.48±0.86	0.28±0.56	0.37±0.55	0.43±0.63	0.35±0.53	0.39±0.55
1.1	1.29±1.45	1.05±1.28	0.96±1.02	0.76±0.72	0.62±0.66	0.61±0.73	1.35±1.68	0.88±1.34	0.66±1.04	0.41±0.72	0.26±0.5	0.33±0.47
1.2	1.35±1.56	1.19±1.33	1.01±1.04	0.7±0.88	0.44±0.69	0.25±0.46	1.72±1.92	1.6±1.98	1.43±1.96	1.13±1.89	0.82±1.62	0.45±0.95
1.3	2.47±1.71	2.29±1.38	1.91±1.1	1.29±0.89	0.79±0.69	0.51±0.58	2.54±1.97	2.4±1.82	2.04±1.58	1.56±1.52	1.37±1.69	1.19±1.74
1.4	2.68±1.88	2.97±1.69	2.39±1.37	1.61±1.12	1.01±0.85	0.66±0.65	2.64±2.26	2.98±2.13	2.63±1.75	1.79±1.63	1.42±1.54	1.18±1.47
1.5	1.13±1.31	1.6±1.59	2.13±1.47	2.4±1.48	2.07±1.48	1.31±1.26	1.01±1.57	1.59±1.97	2.21±2.08	2.79±2.27	2.33±2.16	1.9±2
1.6	0.33±0.93	0.35±0.82	0.85±1.31	2.05±1.85	2.99±2.05	2.85±1.74	0.16±0.73	0.25±0.8	0.6±1.17	1.66±2.2	2.68±2.7	2.97±2.67
1.7	0.1±0.51	0.1±0.41	0.16±0.39	0.5±0.88	1.4±1.57	2.62±2.08	0.01±0.11	0.01±0.13	0.04±0.23	0.2±0.66	0.7±1.43	1.34±1.94
1.8	0.01±0.08	0.01±0.11	0.03±0.15	0.11±0.58	0.15±0.32	0.52±1.05	0±0.13	0±0.05	0.01±0.06	0.01±0.1	0.05±0.38	0.15±0.65
1.9	0.01±0.08	0.01±0.03	0.01±0.06	0.01±0.08	0.04±0.07	0.15±0.24	0±0.05	0±0.02	0±0.04	0±0.02	0±0.06	0.01±0.12
2	0.01±0.05	0±0.02	0±0.03	0±0.02	0±0.02	0.07±0.35	0±0.03	0±0.01	0±0.01	0±0.01	0±0	0.02±0.16
2.1	0.01±0.05	0.01±0.04	0±0.04	0.01±0.05	0.01±0.07	0±0	0±0.06	0±0.01	0±0.01	0±0.03	0±0.02	0±0
2.2	0.02±0.06	0.01±0.04	0.01±0.04	0±0.02	0±0.02	0±0	0.01±0.1	0±0.01	0±0.01	0±0.03	0±0	0±0.03
2.3	0±0.04	0±0.01	0±0.04	0±0.01	0±0.01	0±0	0±0.01	0±0.01	0±0.01	0±0.01	0±0.04	0±0
2.4	0±0.02	0±0.02	0±0.05	0±0.01	0±0.01	0±0	0±0.01	0±0.01	0±0	0±0	0±0.03	0±0
2.5	0±0.11	0±0.07	0±0.07	0±0.07	0±0.1	0±0	0.01±0.07	0±0.02	0±0.01	0±0.08	0±0.02	0±0
GF	Autumn						Winter					
	35 nm	50 nm	75 nm	110 nm	165 nm	265 nm	35 nm	50 nm	75 nm	110 nm	165 nm	265 nm
0.9	0.04±0.17	0.02±0.09	0.02±0.14	0.03±0.13	0.01±0.09	0.14±0.36	0.08±0.23	0.03±0.14	0.02±0.1	0.03±0.14	0.05±0.27	0.56±0.67
1	0.78±0.97	0.75±0.86	1.1±1.05	1.29±1.07	1.01±0.88	0.93±1.02	1.1±1.27	0.93±1	1.04±0.87	0.98±0.92	0.9±0.83	0.85±1.09
1.1	2.06±2.01	1.69±1.68	1.52±1.24	1.03±0.89	0.74±0.71	0.79±0.77	2.16±1.79	1.7±1.54	1.67±1.12	1.08±0.91	0.91±0.79	1±1.03
1.2	1.38±1.39	1.3±1.27	1.02±1.02	0.63±0.83	0.35±0.59	0.21±0.42	1.31±1.17	1.12±0.89	0.93±0.75	0.62±0.63	0.49±0.54	0.35±0.53
1.3	2.47±1.54	2.24±1.35	1.92±1.09	1.44±0.94	0.96±0.81	0.62±0.64	2.07±1.21	1.98±1	1.67±0.74	1.1±0.69	0.87±0.64	0.6±0.58
1.4	2.38±1.78	2.79±1.7	2.16±1.41	1.35±1.3	1.01±1.19	0.77±0.99	2.03±1.56	2.65±1.51	1.44±1.02	0.74±0.79	0.79±0.71	0.68±0.71
1.5	0.68±1.1	1.04±1.22	1.85±1.38	2.69±1.66	2.27±1.81	1.36±1.55	0.76±0.97	1.28±0.98	2.37±1.33	2.29±1.49	1.53±1.57	0.77±1.12
1.6	0.08±0.38	0.1±0.39	0.32±0.61	1.37±1.56	2.97±2.15	3.08±2.24	0.24±0.62	0.21±0.62	0.72±0.79	2.15±1.77	2.82±2.02	2.73±2.24
1.7	0.03±0.12	0.03±0.18	0.04±0.23	0.11±0.37	0.63±1.13	1.69±2.08	0.07±0.42	0.05±0.43	0.06±0.45	0.15±0.45	0.73±1.15	1.91±2.28
1.8	0.01±0.05	0.01±0.09	0.02±0.15	0.01±0.09	0.02±0.15	0.16±0.49	0.02±0.08	0.01±0.05	0.01±0.06	0.11±0.22	0.14±0.28	0.23±0.64
1.9	0.02±0.09	0.01±0.04	0.01±0.07	0.01±0.06	0.01±0.05	0.08±0.38	0.02±0.1	0.01±0.05	0.01±0.06	0.06±0.12	0.05±0.13	0.11±0.27
2	0±0.04	0±0.03	0±0.03	0.01±0.05	0.01±0.07	0.16±0.6	0.01±0.07	0.01±0.07	0±0.04	0.03±0.1	0.09±0.17	0.22±0.4
2.1	0.01±0.06	0±0.02	0±0.03	0.01±0.04	0±0.02	0±0	0.01±0.07	0±0.04	0.01±0.07	0.16±0.26	0.2±0.26	0±0
2.2	0.02±0.09	0±0.02	0±0.02	0±0.02	0±0.01	0±0	0.02±0.08	0.01±0.11	0.01±0.07	0.05±0.12	0.02±0.14	0±0
2.3	0±0.02	0±0.01	0±0.01	0±0.02	0±0.02	0±0	0.01±0.05	0±0.02	0±0.04	0.02±0.07	0.01±0.07	0±0
2.4	0±0.02	0±0.01	0±0.02	0±0.01	0±0.01	0±0	0±0.03	0±0.01	0±0.01	0.02±0.12	0±0.09	0±0
2.5	0.04±0.17	0.01±0.05	0.01±0.05	0.01±0.05	0±0.02	0±0	0±0.14	0.02±0.09	0.02±0.14	0.01±0.46	0.01±0.48	0±0

Hygroscopic properties of the ambient aerosol in southern Sweden

E. O. Fors et al.

Title Page

Abstract

Introduction

Conclusions

References

Tables

Figures

◀

▶

◀

▶

Back

Close

Full Screen / Esc

Printer-friendly Version

Interactive Discussion

Hygroscopic properties of the ambient aerosol in southern Sweden

E. O. Fors et al.

Table 5. CCN closure coefficients for four different supersaturation ratios.

Critical supersaturation, s_c (%)	k ($CCN_{\text{modeled}}/CCN_{\text{measured}}$)	Coefficient of determination, R^2
1	0.95	0.93
0.7	0.93	0.94
0.4	0.84	0.93
0.2	0.74	0.92
0.1	0.76	0.91

Title Page

Abstract

Introduction

Conclusions

References

Tables

Figures

◀

▶

◀

▶

Back

Close

Full Screen / Esc

Printer-friendly Version

Interactive Discussion

Hygroscopic properties of the ambient aerosol in southern Sweden

E. O. Fors et al.

Title Page

Abstract

Introduction

Conclusions

References

Tables

Figures

◀

▶

◀

▶

Back

Close

Full Screen / Esc

Printer-friendly Version

Interactive Discussion

Table 7. Seasonal average CCN concentrations (cm^{-3}) with standard deviations from the DMT CCNC.

s_c (%)	0,1	0,2	0,4	0,7	1
Spring	372±269	751±491	1183±713	1563±865	1828±971
Summer	322±168	792±448	1298±714	1775±879	2093±988
Autumn	291±235	595±511	946±774	1319±1116	1573±1129
Winter	421±267	705±448	973±608	1221±719	1379±785

Hygroscopic properties of the ambient aerosol in southern Sweden

E. O. Fors et al.

Table 8. Properties of seasonal modal fits from averaged DMPS and H-TDMA data. D_i , σ_i , and N_i are the geometric mean mode diameter, the width of the mode, and the number concentration in each mode respectively, where i denotes mode number. ε , which is the modeled volume fraction of dissolved compounds, is based on ammonium sulfate.

	Spring	Summer	Autumn	Winter
D_1 (nm)	7.89	12.36	10.23	9.53
D_2 (nm)	55.47	45.68	50.91	53.77
D_3 (nm)	187.51	135.18	186.26	177.30
σ_1	2.02	2.02	2.02	2.02
σ_2	2.02	1.82	1.85	1.68
σ_3	1.99	1.68	1.60	1.68
N_1 (cm ⁻³)	795.17	1131.68	694.85	205.11
N_2 (cm ⁻³)	2478.31	2260.33	1742.78	1062.06
N_3 (cm ⁻³)	468.77	784.41	356.70	718.84
GF ₁	1.33	1.31	1.30	1.29
GF ₂	1.36	1.33	1.31	1.32
GF ₃	1.52	1.44	1.46	1.49
ε_1	0.42	0.38	0.36	0.34
ε_2	0.41	0.39	0.35	0.36
ε_3	0.61	0.50	0.52	0.56
$\kappa_{p,1}$	0.22	0.21	0.20	0.19
$\kappa_{p,2}$	0.22	0.20	0.18	0.19
$\kappa_{p,3}$	0.30	0.25	0.25	0.28

[Title Page](#)
[Abstract](#)
[Introduction](#)
[Conclusions](#)
[References](#)
[Tables](#)
[Figures](#)
[⏪](#)
[⏩](#)
[◀](#)
[▶](#)
[Back](#)
[Close](#)
[Full Screen / Esc](#)
[Printer-friendly Version](#)
[Interactive Discussion](#)

Hygroscopic properties of the ambient aerosol in southern Sweden

E. O. Fors et al.

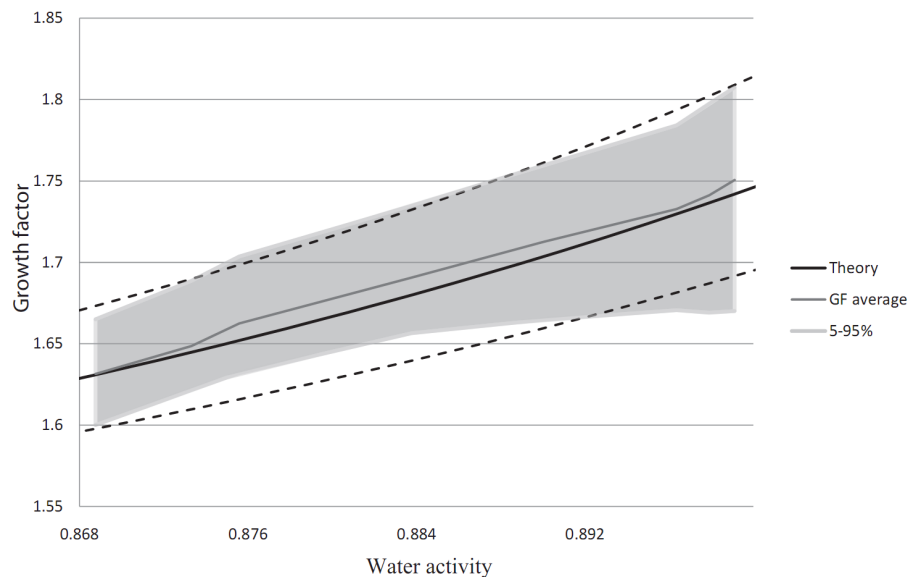


Fig. 1. Growth factor data as function of water activity and particle diameter from automated salt scans for the complete data set. The grey area represents 5% to 95% of the data. Dotted lines represent $\pm 1.2\%$ RH, which is the instrument uncertainty (Nilsson et al., 2009).

[Title Page](#)[Abstract](#)[Introduction](#)[Conclusions](#)[References](#)[Tables](#)[Figures](#)[⏪](#)[⏩](#)[◀](#)[▶](#)[Back](#)[Close](#)[Full Screen / Esc](#)[Printer-friendly Version](#)[Interactive Discussion](#)

Hygroscopic properties of the ambient aerosol in southern Sweden

E. O. Fors et al.

Title Page

Abstract

Introduction

Conclusions

References

Tables

Figures



Back

Close

Full Screen / Esc

Printer-friendly Version

Interactive Discussion

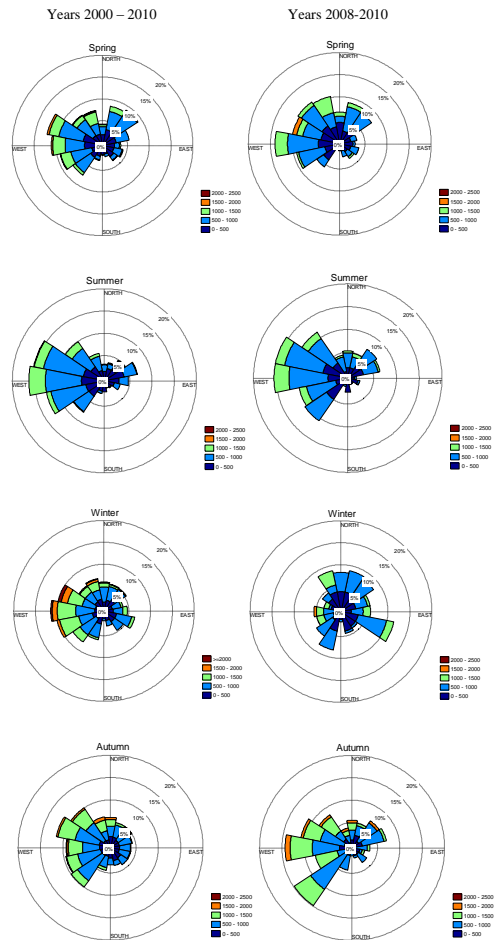


Fig. 2a. Comparison of direction of air center of mass from this data set relative to the period 2001–2010. The trajectories are calculated 72 h backwards. The legend denotes distance to center of gravity in km.

Hygroscopic properties of the ambient aerosol in southern Sweden

E. O. Fors et al.

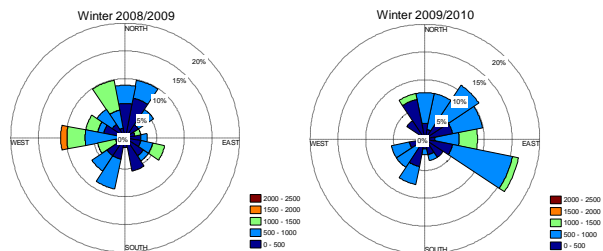


Fig. 2b. Comparison between the winter 2008/2009 and the winter 2009/2010. The legend denotes distance to center of gravity in km.

[Title Page](#)[Abstract](#)[Introduction](#)[Conclusions](#)[References](#)[Tables](#)[Figures](#)[⏪](#)[⏩](#)[◀](#)[▶](#)[Back](#)[Close](#)[Full Screen / Esc](#)[Printer-friendly Version](#)[Interactive Discussion](#)

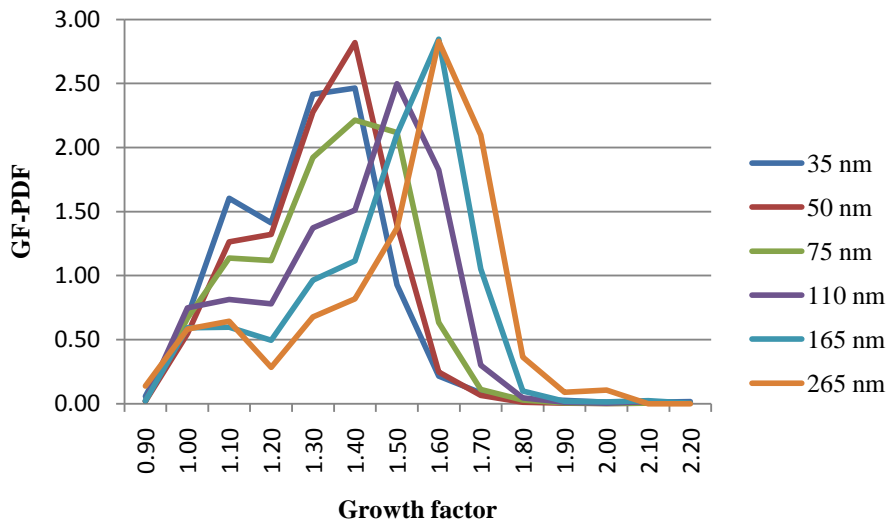


Fig. 3. Mean values of the GF-PDFs for different dry sizes for the entire data set.

Hygroscopic properties of the ambient aerosol in southern Sweden

E. O. Fors et al.

Title Page

Abstract Introduction

Conclusions References

Tables Figures

⏪ ⏩

◀ ▶

Back Close

Full Screen / Esc

Printer-friendly Version

Interactive Discussion



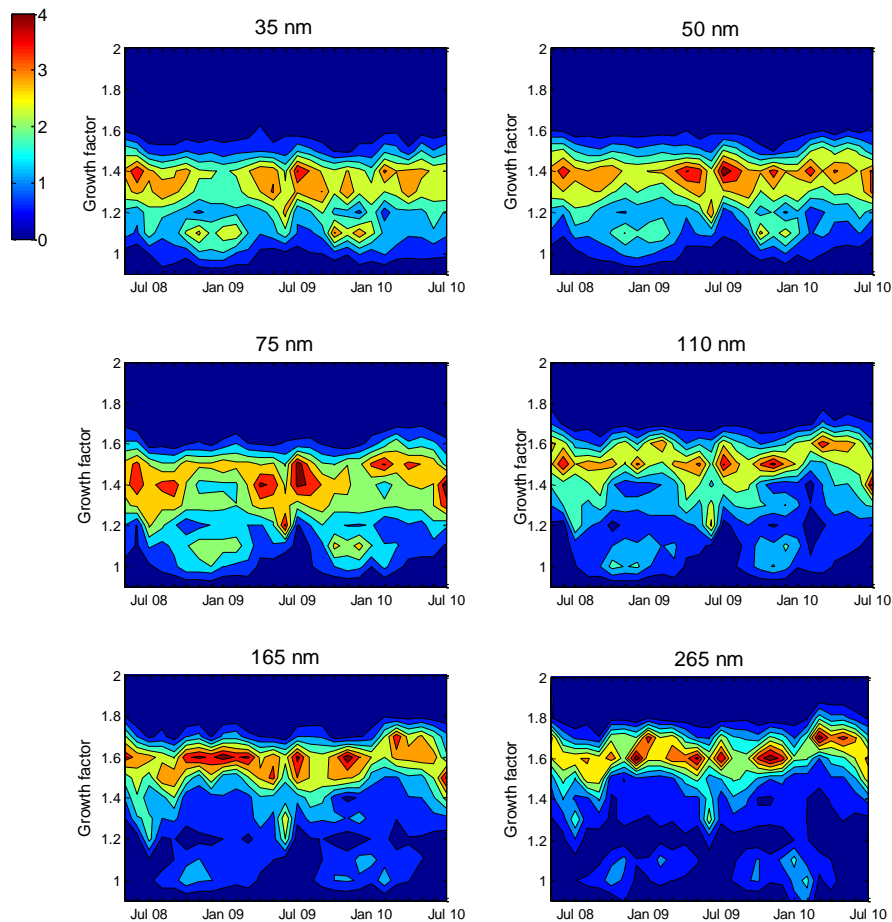


Fig. 4. Linearly interpolated contour plots of the GF-PDFs for different dry sizes based on monthly average values.

Hygroscopic properties of the ambient aerosol in southern Sweden

E. O. Fors et al.

Title Page

Abstract Introduction

Conclusions References

Tables Figures

⏪ ⏩

◀ ▶

Back Close

Full Screen / Esc

Printer-friendly Version

Interactive Discussion



Hygroscopic properties of the ambient aerosol in southern Sweden

E. O. Fors et al.

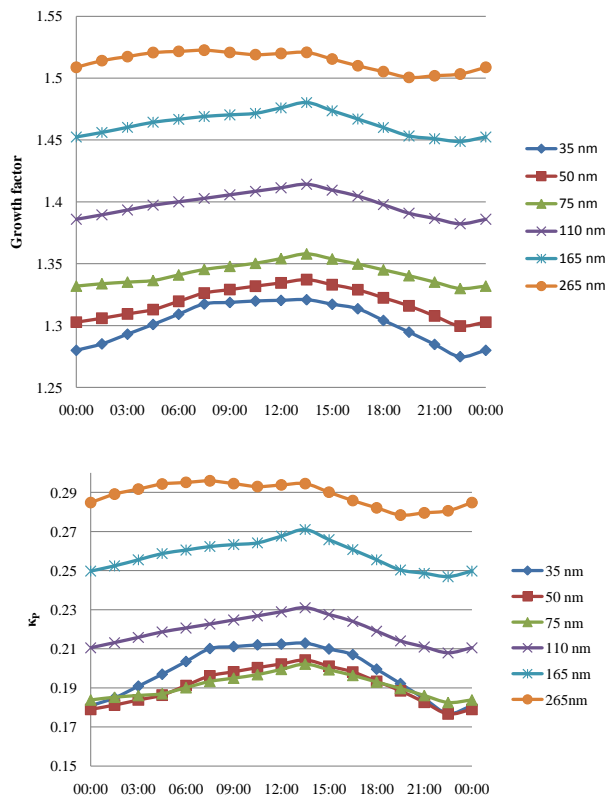


Fig. 5. Diurnal variation for the full data set for the different dry sizes. **(a)** Illustrates the growth factor variation and **(b)** the variation in a κ_p .

Title Page

Abstract Introduction

Conclusions References

Tables Figures

◀ ▶

◀ ▶

Back Close

Full Screen / Esc

Printer-friendly Version

Interactive Discussion



Hygroscopic properties of the ambient aerosol in southern Sweden

E. O. Fors et al.

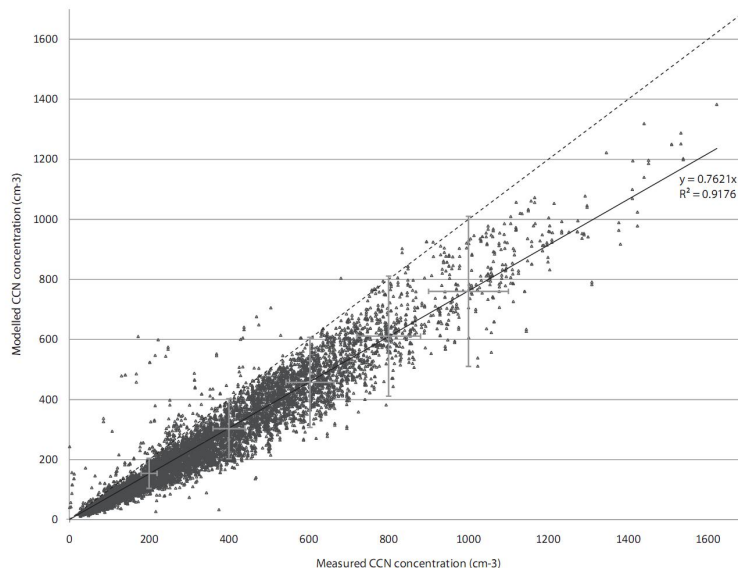


Fig. 6. Correlation between measured and modeled CCN concentrations for 0.1% supersaturation. The model slightly underpredicts the number of CCN, and the tendency is increasing with decreasing s_c . The dotted line is the 1:1 line, and the grey error bars represent a 10% relative uncertainty in the s from the CCNC (x-axis) and the error propagation described in Sect. 4.6 (y-axis) respectively.

[Title Page](#)[Abstract](#)[Introduction](#)[Conclusions](#)[References](#)[Tables](#)[Figures](#)[⏪](#)[⏩](#)[◀](#)[▶](#)[Back](#)[Close](#)[Full Screen / Esc](#)[Printer-friendly Version](#)[Interactive Discussion](#)

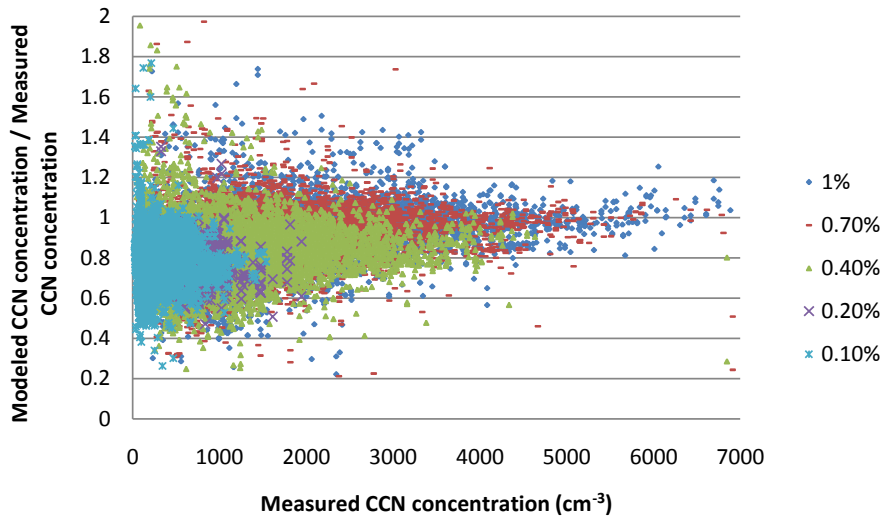


Fig. 7. Ratio of modeled to measured CCN concentration for five different s ratios.

Hygroscopic properties of the ambient aerosol in southern Sweden

E. O. Fors et al.

Title Page

Abstract Introduction

Conclusions References

Tables Figures

⏪ ⏩

◀ ▶

Back Close

Full Screen / Esc

Printer-friendly Version

Interactive Discussion



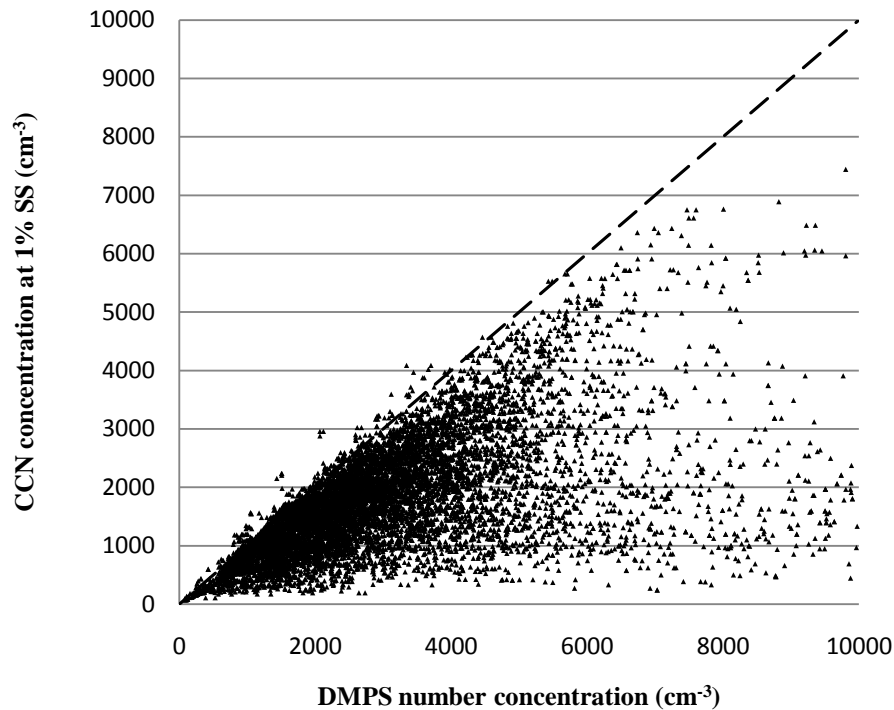


Fig. 8. Particle concentration from DMPS and CCNC measuring at 1% s. The dotted line is the 1:1-line.

Hygroscopic properties of the ambient aerosol in southern Sweden

E. O. Fors et al.

Title Page

Abstract Introduction

Conclusions References

Tables Figures

◀ ▶

◀ ▶

Back Close

Full Screen / Esc

Printer-friendly Version

Interactive Discussion



Hygroscopic properties of the ambient aerosol in southern Sweden

E. O. Fors et al.

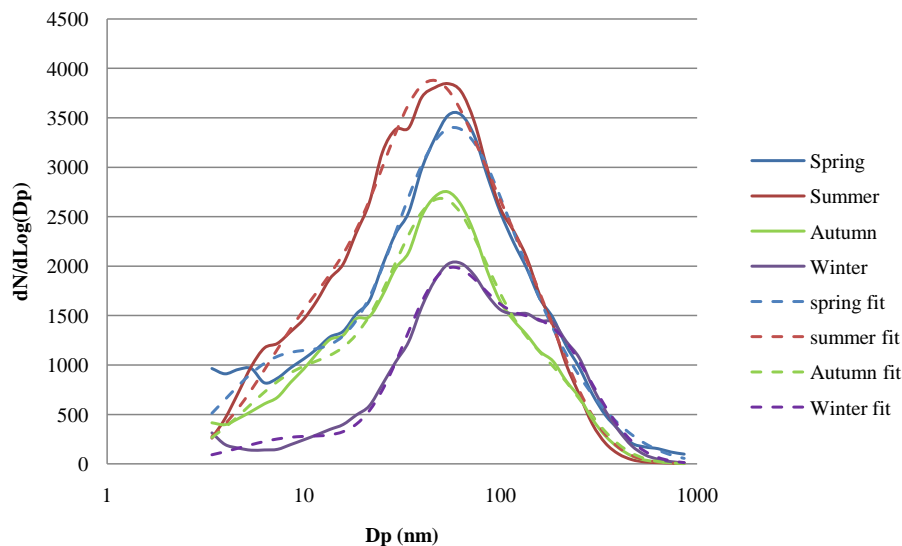


Fig. 9. Seasonal average size distributions from DMPS data and three mode log-normal fits.

[Title Page](#)[Abstract](#)[Introduction](#)[Conclusions](#)[References](#)[Tables](#)[Figures](#)[◀](#)[▶](#)[◀](#)[▶](#)[Back](#)[Close](#)[Full Screen / Esc](#)[Printer-friendly Version](#)[Interactive Discussion](#)

Hygroscopic properties of the ambient aerosol in southern Sweden

E. O. Fors et al.

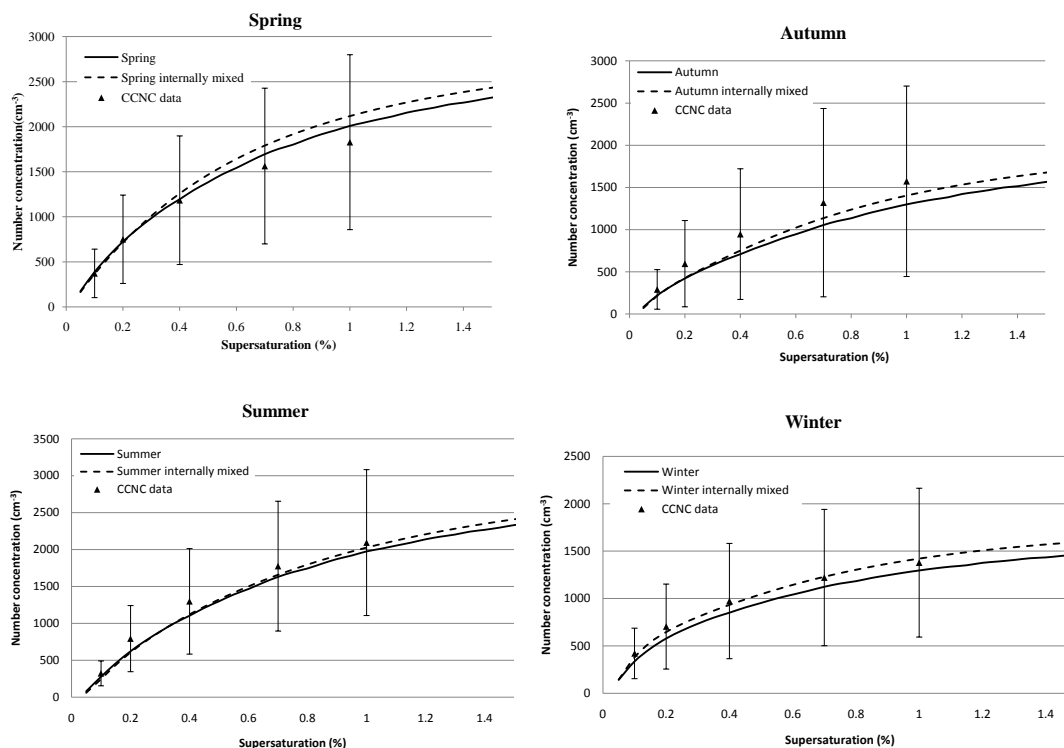


Fig. 10. Average measured CCN concentrations as a function of season and s_c denoted with symbols, and modeled values (internally and externally mixed) derived from averaged DMPS and H-TDMA data for the respective seasons. The error bars are standard deviations from the CCNC data.

[Title Page](#)[Abstract](#)[Introduction](#)[Conclusions](#)[References](#)[Tables](#)[Figures](#)[◀](#)[▶](#)[◀](#)[▶](#)[Back](#)[Close](#)[Full Screen / Esc](#)[Printer-friendly Version](#)[Interactive Discussion](#)